Two-Tiered Transition of the North Atlantic Surface Hydrology during the Past 1.6 Ma: Multiproxy Evidence from Planktic Foraminifera

Authors: Yamasaki, Makoto, Shimada, Chieko, Ikehara, Minoru, and Schiebel, Ralf

Source: Paleontological Research, 25(4) : 345-365

Published By: The Palaeontological Society of Japan

URL: https://doi.org/10.2517/2020PR026

Paleontological Research, vol. 25, no. 4, pp. 345–365, October 1, 2021

doi:10.2517/2020PR026

Two-tiered transition of the North Atlantic surface hydrology during the past 1.6 Ma: multiproxy evidence from planktic foraminifera

MAKOTO YAMASAKI[1], CHIEKO SHIMADA[2,3], MINORU IKEHARA[4] AND RALF SCHIEBEL[5]

[1]*Department of Earth Resource Science, Graduate school of International Resource Sciences, Akita University, Tegata-Gakuenmachi 1-1, Akita-shi, Akita 010-8502, Japan (e-mail: yamasaki@gipc.akita-u.ac.jp)*
[2]*Department of Geology and Paleontology, National Museum of Nature and Science, Amakubo 4-1-1, Tsukuba-shi, Ibaraki 305-0005, Japan*
[3]*Research Institute of Geology and Geoinformation, National Institute of Advanced Industrial Science and Technology (AIST), Higashi 1-1-1, Tsukuba-shi, Ibaraki 305-8567, Japan*
[4]*Center for Advanced Marine Core Research (CMCR), Kochi University, Monobe-Otsu 200, Nankoku-shi, Kochi 783-8502, Japan*
[5]*Climate Geochemistry, Max Planck Institute for Chemistry, Hahn-Meitner-Weg 1, 55128 Mainz, Germany*

Received November 10, 2019; Revised manuscript accepted July 3, 2020

Abstract. Analyses of planktic foraminiferal assemblage data, test morphology, and stable oxygen isotopes from the Integrated Ocean Drilling Program (IODP) Site U1304 in the North Atlantic reveal a stepwise regional migration of the oceanic fronts around 0.6 Ma and 0.4 Ma, i.e., during Marine Isotope Stages (MISs) 15 and 11, respectively. Both changes of planktic foraminiferal assemblages and shell carbonate isotopes indicate that the cold Arctic waters in general persisted at IODP Site U1304 from 1.6 to 0.6 Ma (MIS 15), even though the warmer waters originating from the Atlantic waters episodically bathed Site U1304 during the interglacial periods. During the time-interval from *ca.* 0.6 to 0.4 Ma (MISs 15–11), an alternating dominance of Artic and Atlantic waters at the Site U1304 has been suggested from isotopic evidence. In MIS 11, the dominant planktic foraminiferal species *Neogloboquadrina pachyderma* experienced a short-term but significant decrease in test size. The test-size change may have been caused by accelerated reproduction in more favorite feeding conditions over the long-lasting interglacial period around the Subarctic Front. This finding is supported by the presence of massive diatoms oozes in the same time-interval. The modern-type glacial/interglacial change of the surface water system established since *ca.* 0.4 Ma (MIS 11) followed the Mid-Brunhes Event.

Keywords: North Atlantic, Pleistocene, stable isotopes, Subarctic Front, test morphometry

Introduction

In 2004, Integrated Ocean Drilling Program (IODP) Expedition 303 successfully penetrated a unique lithofacies of thinly-laminated diatomaceous oozes, occurring sporadically but repeatedly spanning the last 1.6 million years (Channell *et al*., 2006; Expedition 303 Scientists, 2006; Shimada *et al*., 2008). These monospecific diatomaceous oozes at the Site U1304 are believed to be a consequence of mass dumping of monospecific diatom frustules around the Subarctic Front (= Subarctic Convergence), a narrow zone between the colder and warmer surface water masses originating from the Labrador Sea and the North Atlantic Current, respectively (Bodén and Backman, 1996). Temporal variability in the advance and retreat of oceanic fronts between different water masses gives promising insights into the detailed paleoceanographic evolution. However, timing of large-scale migrations of such oceanic fronts is still under debate for the North Atlantic. Considering these points, paleoceanographic data from the Site U1304 add new information for a better reconstruction of the past oceanic fronts in the North Atlantic.

In the modern hydrographic setting, deep-water formation mainly occurs in the North Atlantic, the Labrador and Greenland Seas (Marshall and Schott, 1999), and in the Weddell Sea, Antarctica (Gordon, 1982). Particularly, the formation of such dense waters during winter in the Greenland and Norwegian Seas has an important role for the distribution of the water masses in the world ocean (Swift, 1986). Therefore, previous investigations have presented many ideas on the evolution in the surface water masses introducing various paleoceanographic proxies (e.g. McManus *et al.*, 1994; Oppo and Lehman, 1995;

Wright and Flower, 2002; Oppo *et al*., 2006; Alonso-Garcia *et al*., 2011; Barker *et al*., 2015; Mokeddem and McManus, 2016). The calcareous tests of planktic foraminifera are a major archive from which these proxies are analyzed as an essential source of data for surface ocean reconstruction (e.g. Ruddiman and Glover, 1975; Alonso-Garcia *et al.*, 2011; Kandiano *et al*., 2012; Husum and Hald, 2012; Barker *et al*., 2015; Mokeddem and McManus, 2016). As a proxy of the high latitude ocean, *Neogloboquadrina pachyderma* (Ehrenberg) has played a particularly important role for decoding of the past surface ocean conditions because the species dominates the planktic foraminiferal communities in the (sub-) polar oceans, such as the oceanic waters of the Greenland and the Labrador Seas (e.g. Bé, 1960; Bé and Tølderlund, 1971; Hillaire-Marcel and Bilodeau, 2000; Hillaire-Marcel *et al*., 2001, 2004, 2008; Pados and Spielhagen, 2014; Schiebel *et al.*, 2017).

The overall test size of the combined planktic foraminiferal assemblage is believed to have gradually increased over the Cenozoic Era, and maximized at the most favorable conditions (Schmidt *et al*., 2003, 2004). An increase in size of *N. pachyderma* at 1.1–1.0 Ma in the Norwegian-Greenland Seas may reflect their evolutionary adaptation when cold waters progressively appeared in the high latitudes together with intensifying glaciations since the middle Pleistocene Epoch. Huber *et al.* (2000) and Kucera and Kennett (2002) found a synchronous test size increase of *N. pachyderma* in the North Pacific, and claimed that "the modern type" of the species had appeared since *ca.* 1 Ma. In the western North Atlantic, such increases in *N. pachyderma* test size paused around the middle Pleistocene time (Yamasaki *et al.*, 2008). Möller *et al.* (2013) show a strong linear correlation between the mean shell size and sea surface temperature (SST) in the Arctic region where the summer SST is less than 9 °C, and propose test size as a tool for the reconstruction of past SSTs from fossil individuals. In addition, multi-species oxygen isotope data allow decoding of the past ocean stratification and possibly seasonality (Hillaire-Marcel and Bilodeau, 2000; Simstich *et al.*, 2003; Hodell *et al.*, 2009; Jonkers *et al*., 2010, 2013). In this paper, we have analyzed the assemblage composition, test morphology, and stable oxygen isotopes of planktic foraminifera shells as proxies of high latitudinal paleoceanography, and discuss the surface ocean conditions of the past 1.6 million years in the North Atlantic, particularly focusing on temporal and spatial variability in the oceanic fronts, using the sediment core material from the IODP Site U1304.

Surface hydrology

The Site U1304 is situated south of Greenland (Figure 1). The subpolar North Atlantic is characterized by a counter clockwise circulation. In the eastern and central part of the ocean, the warm North Atlantic Currents and flows northward turning into the Irminger Current (Meincke, 2002). The westward West Greenland Current and the surface waters of Baffin Bay converge in the Labrador Current off the east coast of Canada and compose the counter clockwise Subarctic Gyre with the Subarctic Front at its northeastern limit (Ruddiman and Glover, 1975; Meincke, 2002). The surface waters of the Nordic Seas include three water bodies, (1) the coastal Polar waters sourced from surface waters of the Arctic Ocean, (2) the Atlantic waters originating from the warm North Atlantic Current, and (3) the intermediate Arctic waters (Swift, 1986; Fogelqvist *et al*., 2003). The boundary of the former two Polar and Atlantic waters is defined as the Polar Front, and the limit between the latter two Atlantic and Arctic waters is the Arctic Front (Swift, 1986; Hald, 2001; Risebrobakken *et al*., 2005). The Subarctic Front, or Subpolar Front, delimits the North Atlantic Current (NAC) from the colder northwestern water bodies (Figure 1). Today, the studied Site U1304 is located at the proximity of the Subarctic Front and experiences an advection of Atlantic waters from the south. The overflows from the Nordic Seas are a major source for the deep waters to the North Atlantic, namely North Atlantic Deep Water (NADW), and thus are important contributors to the Atlantic Meridional Overturning Circulation (Eldevik *et al*., 2005; Repschläger *et al*., 2015).

During the Last Glacial Maximum, deep-water circulation patterns were noticeably different from the modern oceanic settings. The Norwegian Sea is the dominant source of deep water in the North Atlantic during interglacial conditions, when the Polar Front is close to the coast of Greenland. As soon as ice accumulates over the northern continents, and the Polar Front takes a more southern position, sinking of surface waters occurs in the northern Atlantic rather than in the Norwegian Sea (Duplessy *et al*., 1988). More recently, during the Last Glacial Maximum, NADW shoaled to form Glacial North Atlantic Intermediate Water (GNAIW) originated from the upper water column of the Nordic Seas (Howe *et al*., 2016; Matsumoto, 2017) and overflows were at least intermittently present even in glacial time-periods (Crocket *et al*., 2011).

Material and methods

Samples were obtained from the IODP Site U1304 (53°03.40'N, 33°31.78'W; water depth 3024 m), located at the southern limit of the Gardar Drift (Figure 1), just to the north of the Charlie Gibbs Fracture Zone (Expedition 303 Scientists, 2006). Lithology of U1304 is characterized by an episodic occurrence of diatomaceous oozes,

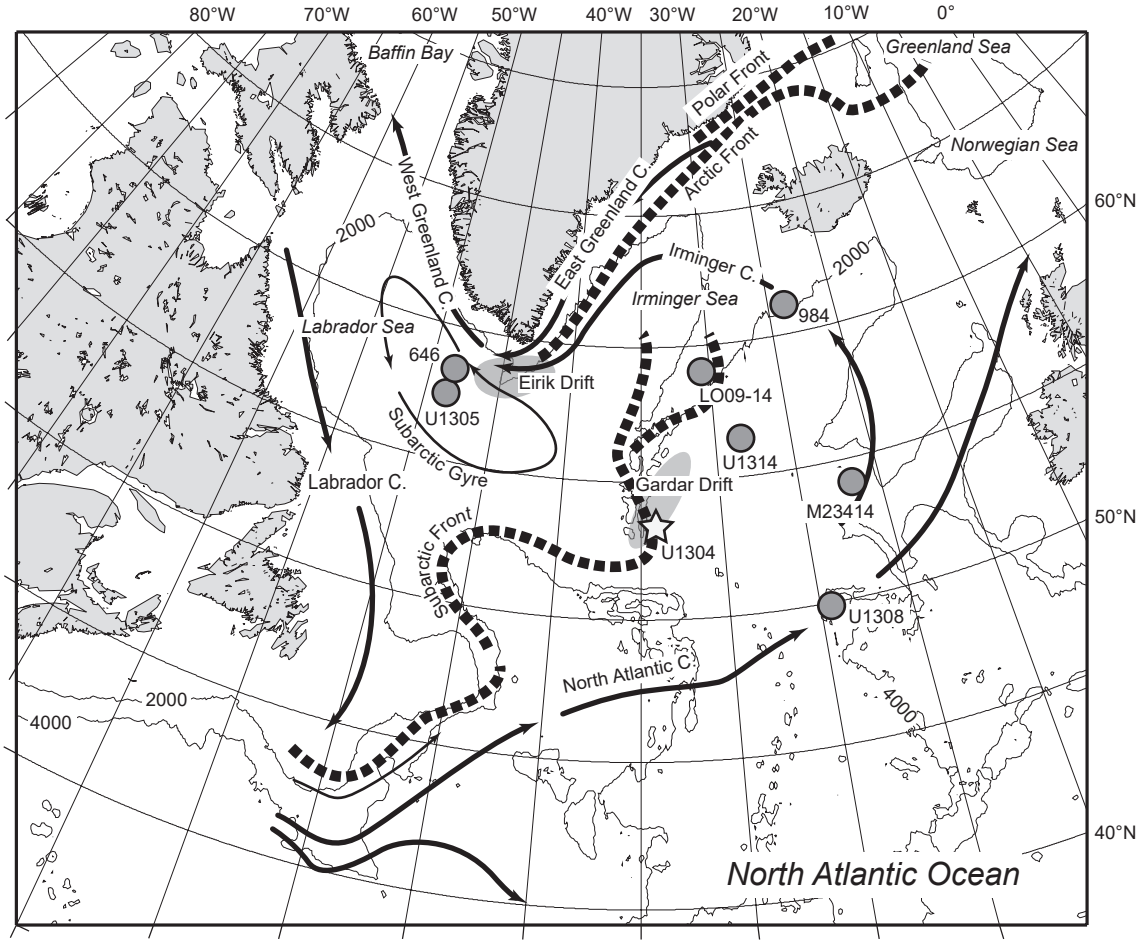

Figure 1. Map showing the IODP Site U1304 and related sites. Dark colored circles show the drilled sites. Surface ocean currents and fronts from Ruddiman and Glover (1975) and Swift (1986). Dotted lines indicate the Polar Front, Arctic Front and Subarctic Front.

mainly consisting of a single araphid marine planktic diatom species, *Thalassiothrix longissima* Cleve and Grunow throughout the studied section (Channell *et al*., 2006; Shimada *et al*., 2008). Less abundant but exceptionally well-preserved calcareous shells of planktic foraminifera are present through the studied section of the core. Similar monospecific *Thalassiothrix* dominances were also observed in the lower Pleistocene (IODP Site U1314, Hayashi and Ono, 2019) and Holocene deposits (LO09-14; Andersen *et al.*, 2004), both being located northeast of the Site U1304.

An age model for the Site U1304 has recently been updated based on oxygen isotope stratigraphy using benthic foraminiferal shells and relative paleointensity data spanning the past 1.5 million years (Xuan *et al.*, 2016). Employing the paleomagnetostratigraphic age model (Expedition 303 Scientists, 2006), we infer a geologic age of 1.6 million years for the oldest sample analyzed in this study.

For planktic foraminiferal assemblage analyses, 243 horizons were analyzed down to 238 m in composite depth (mcd) from the holes U1304A and U1304B (Appendix 1). Samples are from 0.5–2.0 m core depth intervals. The resulting mean temporal resolution lies at 7,000 years (minimum 2,000 years, maximum 48,000 years). Due to the relatively low temporal resolution we cannot discuss the relationships between each of the glacials and interglacials in detail. Therefore, focus of this study is on the long-range environmental change spanning the past 1.6 million years in terms of changes of oceanic frontal position in the North Atlantic.

Each 10 cm^3 sediment sample was first soaked in a 3% hydrogen peroxide solution for a few hours, then washed through a 63 μm screen, and the retained particles were dried at 60 °C. The size fraction larger than 63 μm was split into smaller aliquots with a micro-splitter, and sieved through a 125 μm screen. Planktic foraminiferal shells larger than 125 μm were picked from the aliquots

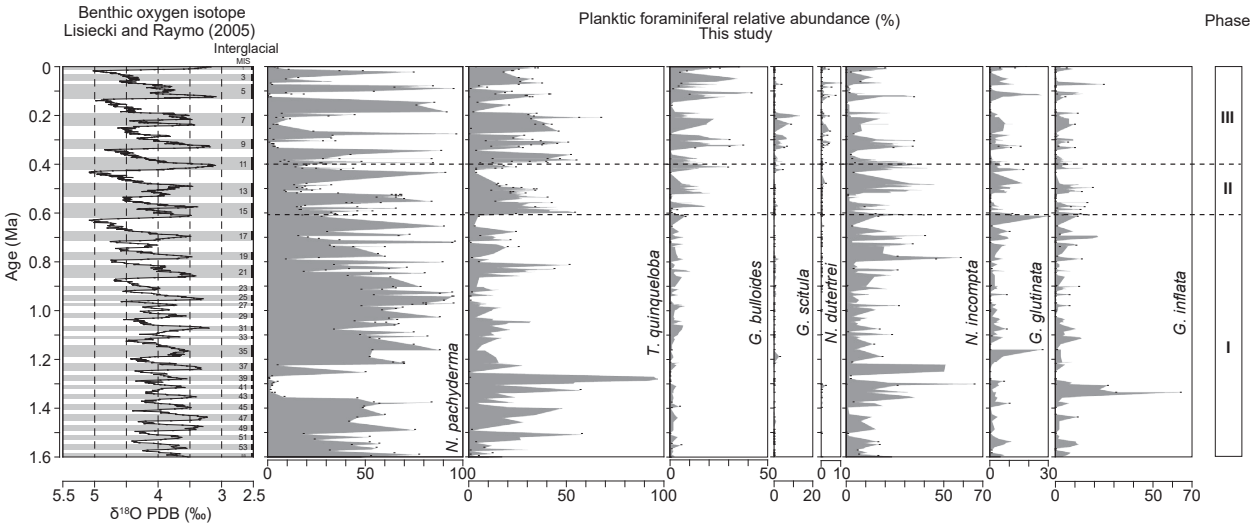

Figure 2. Relative abundance of major planktic foraminifera species from the Site U1304, in comparison to the LR04 (Lisiecki and Raymo, 2005) stack, and Phases I to III.

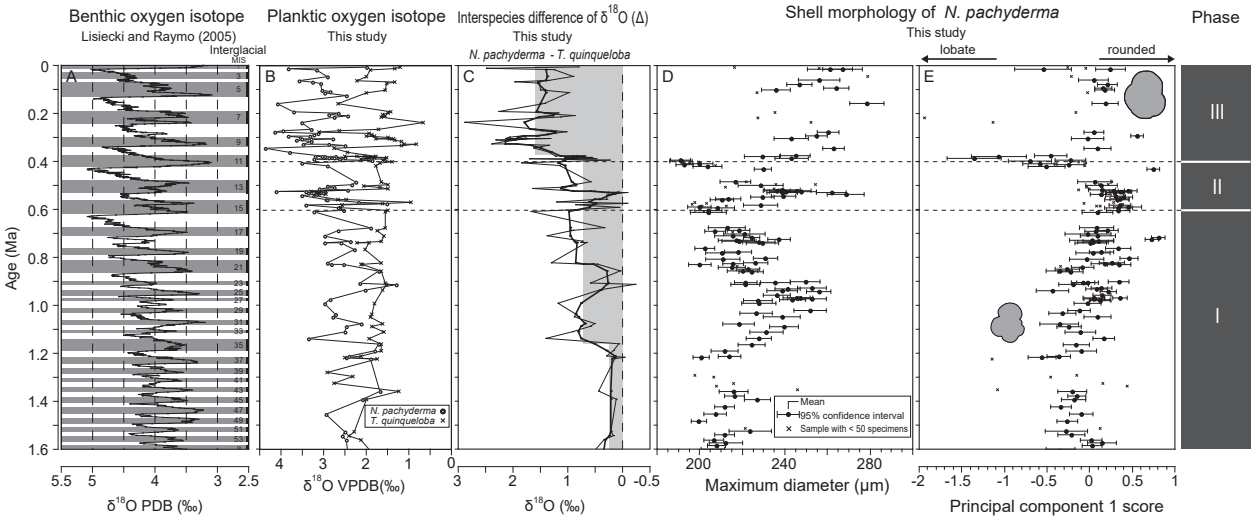

Figure 3. Temporal change of oxygen isotope ratio measured on multiple species of planktic foraminifera and morphology of *N. pachyderma* at the Site U1304. **A,** benthic oxygen isotope LR04 stack (Lisiecki and Raymo, 2005). **B,** open circle, *N. pachyderma*; cross, *T. quinqueloba*. **C,** temporal change of oxygen isotope ratios of the foraminiferal species; thin line, subtracted of *T. quinqueloba* from that of *N. pachyderma*; thick line, three-point running mean; shaded area, mean value during the selective intervals (see the text). **D,** maximum diameters of *N. pachyderma*. **E,** filled circle, PC1 scores of the species; horizontal bar, 95% confidence intervals; cross, horizons consisting of less than 50 specimens.

until -ideally- more than 200 specimens were collected (e.g. Sato *et al*., 2008), identified, counted (Figure 2 and Appendix 1), and morphometrically analyzed (Figures 3 to 5).

Stable oxygen isotope ($\delta^{18}O$) measurements of the calcareous shells of *N. pachyderma* and *Turborotalita quinqueloba* (Natland) were conducted at 103 horizons in the Center for advanced Marine Core Research (CMCR), Kochi University, Japan, using a dual inlet IsoPrime Mass Spectrometer (GV Instruments Co.) equipped with an automated carbonate system (Figure 3B and Appendix 2). The measurements were performed on an average of 17 and 70 specimens of *N. pachyderma* and *T. quinqueloba*, respectively. All of the shells were hand-picked within 150–250 μm size fraction. The specimens were then soaked in methanol with a brief ultrasonic cleaning

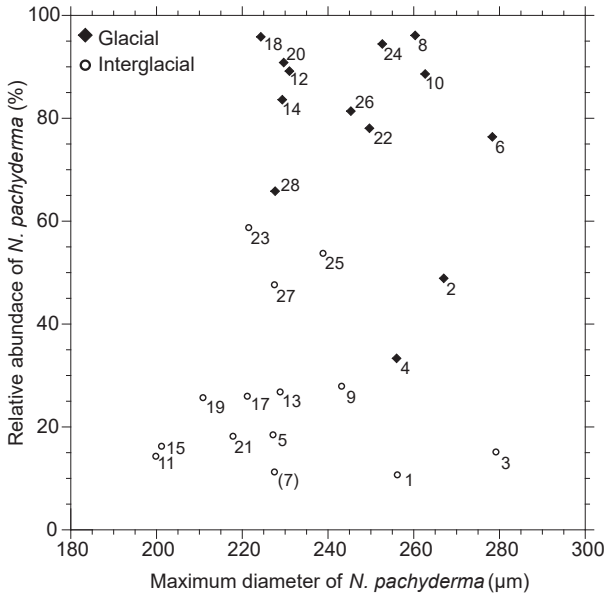

Figure 4. Comparison between the maximum diameter and relative abundance of *N. pachyderma* over the past 1 million years at the Site U1304. Numbers show Marine Isotope Stages (MISs); filled diamonds, the glacial periods; open circles, the interglacial periods. The data point on MIS 7 is given in parentheses because the sample contains less than twenty specimens of *N. pachyderma*. Note that our sparse sampling intervals do not necessarily provide full glacial and interglacial conditions within each Marine Isotope Stages.

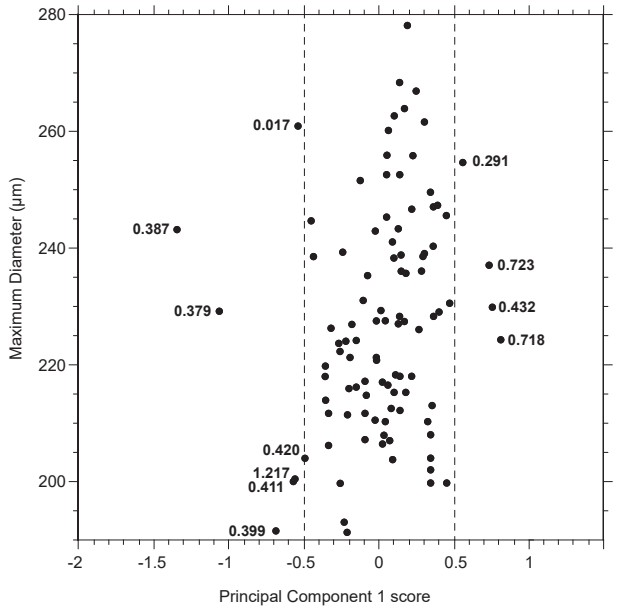

Figure 5. Comparison of the maximum diameter of *N. pachyderma* and PC1 score at the Site U1304. Numbers show ages (Ma) for the outlier samples which involve >0.5 and/or <−0.5 of PC1 score.

to remove adherent particles. Isotopic data are relative to the Vienna Pee Dee Belemnite (VPDB) standard, established via the NBS 19 calcite standard. Overall analytical reproducibility calculated from replicate measurements of the standard carbonate was better than ± 0.1‰ (± 1σ).

We have employed the mean maximum diameter to analyze changes in the *N. pachyderma* test morphology, which enables direct comparison with the previous works of Huber *et al*. (2000), Kucera and Kennett (2002), and Yamasaki *et al.* (2008). From these comparisons, we can correlate their size differences between northeastern Pacific and the north Atlantic. From the work of Yamasaki *et al.* (2008) on the same Site U1304, *N. pachyderma* test size data from 105 samples have been included in this paper. New measurements of *N. pachyderma* test size have been carried out on 138 samples (Figure 3D and Appendix 3). Morphological measures of each specimen were obtained using the automated image analyses system at Université d'Angers, France (Schiebel and Movellan, 2012; Schiebel and Hemleben, 2017). All specimens of *N. pachyderma* were oriented in the standard taxonomic umbilical view to measure (1) maximum diameter, (2) aspect ratio, (3) shape factor, and (4) convexity of the individual tests (Appendix 3). In the case of very low *N. pachyderma* abundance at any horizon, a second aliquot was used for additional specimens. In our analyses, two distinct ultrastructural morphotypes of *N. pachyderma* were analyzed, the crystalline and the reticulate shells (Kennett and Srinivasan, 1980). In total, 16,576 specimens were measured. Principal component analyses (PCAs) were employed to confirm the temporal trend of morphological variability that comprises aspect ratio, shape factor, and convexity in *N. pachyderma* tests using SPSS Statistics 22 (IBM Co.).

Differentiation between the dextral coiling *N. incompta* (Cifelli) and the sinistral *N. pachyderma* had been confirmed by means of molecular genetics by Darling *et al*. (2006), acknowledging the presence of <3% sinistral specimens in *N. incompta*. In this paper, data from exclusively sinistral tests of *N. pachyderma* have been included in the morphometric analyses.

Results

Temporal variability of faunal assemblages

In our analysis, 29 planktic foraminiferal species were identified. Of the total census count, 96.9% was contributed by eight species (Figure 2 and Appendix 1). Major species throughout the analyzed time-interval are *N. pachyderma* and *T. quinqueloba*, while *N. incompta*, *Globigerina bulloides* d'Orbigny, *Globorotalia inflata* (d'Orbigny), *Globigerinita glutinata* (Egger), *Globoro-*

talia scitula (Brady) and *Neogloboquadrina dutertrei* (d'Orbigny) occurred at moderate to minor abundances.

Based on the stratigraphic development of species assemblages, we differentiate between three phases (Figure 2).

Phase I from about 1.6–0.6 Ma (the bottom of the sediment core at 238–115 mcd) is characterized by dominance of a single species, *N. pachyderma,* with abundance spikes of *T. quinqueloba* and *G. inflata* at 197.58 mcd (1.28 Ma) and 207.54 mcd (1.34 Ma), respectively. Relative abundances of *N. pachyderma* generally vary in a quasi-periodical way. During the glacial periods, *N. pachyderma* occurred at more than 70% of the assemblage, and 50% during the interglacial periods in Phase I. In the interglacial time-periods, its abundance gradually decreased from *ca.* 0.8 Ma to 0.6 Ma.

Phase II from 0.6–0.4 Ma (*ca.* 115–61 mcd) is still characterized by a predominance of *N. pachyderma* especially in the glacial time periods. In the interglacial periods, relative abundance of the species dropped to around 20%. Phase II starts with a dominance of *T. quinqueloba* with a maximum abundance (54.2%) at 115.09 mcd (0.59 Ma). *Globigerina bulloides* occurred in minor numbers sometimes exceeding 10% during Phase II.

Phase III from 0.4 Ma–Recent (*ca.* 61–0 mcd) covers the middle to latest Pleistocene near the core top, and is characterized by a high-amplitude variability of *N. pachyderma* occurrence ranging from 0 to 96.2%. During most of the interglacial periods, relative abundances of *N. pachyderma* are below 10%, associating with offsetting abundances of the temperate to subtropical water indicators, *G. bulloides*, *G. scitula,* and *N. dutertrei*, with maximum relative abundances of 37.2%, 5.3%, and 2.7%, respectively. During the early Phase III (MIS11; *ca.* 54–63 mcd), relative abundances of *T. quinqueloba* are high in some horizons as well (Figure 2), and then account for 55.0% of the assemblage at 56.76 mcd (0.38 Ma).

Differential variabilty in the $\delta^{18}O$ of *N. pachyderma* and *T. quinqueloba*

Stable oxygen isotope data of *N. pachyderma* range between 1.30‰ and 4.36‰, getting heavier from the bottom to the core top. $\delta^{18}O$ values of *T. quinqueloba* vary between 0.65‰ and 3.28‰ throughout the studied section, and show larger amplitude during Phases II and III (above 115 mcd, 0.6 Ma) than Phase I (Figure 3B). The $\delta^{18}O$ values of *N. pachyderma* are generally heavier than that of *T. quinqueloba* throughout the studied section with few exceptions (Appendix 2 and Figure 3B). The interspecies difference of the $\delta^{18}O$ values between *N. pachyderma* and *T. quinqueloba* ($\Delta\delta^{18}O_{Npachy\text{-}Tquin}$) ranges from −0.23 to 2.86‰, with heavier values and higher amplitudes toward the younger horizons, in particular from 0.6 Ma (above 115 mcd; Figure 3C). A stepwise $\Delta\delta^{18}O_{Npachy\text{-}Tquin}$ increase seems to be two-tiered from about 0.2‰ on average from MIS 55 at 1.6 Ma (bottom of the core) to 1.16 Ma (186.58 mcd), to 0.8‰ until MIS 11 at 0.4 Ma (61.37 mcd), and 1.6‰ until the Holocene (Figure 3C). The latter of these two steps at MIS 11 seems to be synchronous to the above-described limit between the Phases II and III of the planktic foraminiferal assemblage compositions (Figure 2).

Neogloboquadrina pachyderma test size development

The maximum diameter of *N. pachyderma* tests over the past 1.6 million years ranges from about 210 μm to 270 μm (Figure 3D). Overall, *N. pachyderma* tests are larger in the glacials than interglacials. Largest maximum diameters of *N. pachyderma* > 255 μm occur during the most recent glacials MISs 10 to 2, and interglacials MISs 3 and 1 (Figure 4).

In detail, maximum test diameter of *N. pachyderma* on average is as small as 217 μm near the bottom of the analyzed section (238.01 mcd; 1.6 Ma), and increases to an average of 267 μm at the youngest horizon (3.87 mcd; 16 ka). In a first major step starting from 1.14 Ma (183.86 mcd) test size increases to 250 μm at 0.9 Ma (149.97 mcd). A sudden drop in test size to 200 μm at 0.83 Ma (143.93 mcd) is followed by a time-interval of size changes under 40 μm (> 200 μm to < 240 μm). From 0.54 Ma (101.68 mcd), test size rapidly increases to 269 μm and decreases to a minimum of 191 μm at 0.4 Ma (61.37 mcd). Finally, test size increases again, and remains large after 0.4 Ma.

The long-term change of *N. pachyderma* morphology is expressed by principal component analysis (PCA) employed on the morphometric characteristics of aspect ratio, shape factor, and convexity, using SPSS Statistics 22 (Figure 3E). The first principal component (PC1) explains 70.3% of the total variation in the data. More positive scores account for a more rounded test shape, and more negative score for a more lobate test shape. From 1.6 to 0.78 Ma, more negative scores were observed, and scores turn more positive after 0.78 Ma. Minimum scores (−1.36) at 0.39 Ma (58.26 mcd) are characterized by elongate-shaped specimens of *N. pachyderma*, mostly comprising morphotype *Nps-1* (Eynaud *et al*., 2009) and minor amounts of the "nonencrusted form" (fig. 4a in Kohfeld *et al*., 1996), after which test shapes change from more elongate to more round, including morphotypes *Nps-2*, *3*, and *4* (Eynaud *et al*., 2009), and "encrusted forms" (fig. 4c in Kohfeld *et al*., 1996), throughout the upper part of the studied section. However, average maximum diameter of *N. pachyderma*, i.e., size, is the most distinctive measure of morphometric changed over time; in comparison, the majority PC1-scores as a mea-

sure of shape are within a narrow range between −0.5 and 0.5 (Figure 5), with some exceptions. Since negative PC1 scores involve high aspect ratio and high convexity (Appendix 3), more lobate tests are represented (outline of test is shown in Figure 3E). On the other hand, positive PC1 scores represent more rounded tests. Most of these exceptions are from the short time-interval from 0.43–0.38 Ma (72.43–55.76 mcd) with negative PC1 scores (more lobate tests) including Termination V and the MIS 11.

Discussion

The paleoceanographic changes over the past 1.6 Ma in the following are discussed for three Phases I to III, from 1.6–0.6 Ma, 0.6–0.4 Ma, and 0.4 Ma until the Holocene, respectively. These Phases are deduced from changes in planktic foraminiferal proxies, and supported by earlier sedimentological findings, in particular the temporal distribution of diatom oozes at IODP Site U1304 (Shimada *et al*., 2008).

Phase I, 1.6–0.6 Ma, MIS 55–15

Phase I is characterized by the dominance of *N. pachyderma* and associated (10–20%) *T. quinqueloba* (Figure 2). Since the mid Pleistocene around 1.1–1.0 Ma, *N. pachyderma* had fully achieved evolutionary adaptation in high latitudinal seas under the intensified glaciation (Huber *et al.*, 2000; Kucera and Kennett, 2002). Dominance of *N. pachyderma* in the planktic foraminiferal community characterizes high latitude waters and underlying sediments in the Greenland, Iceland, and Norwegian Seas (GINS) and Labrador Sea, including habitats near the seasonal sea ice (e.g. Bé, 1960; Bé and Tølderland, 1971; Johannessen *et al.*, 1994; Carstens *et al*., 1997; Volkmann, 2000; Schröder-Ritzrau *et al*., 2001; Spielhagen *et al.*, 2011; Schiebel *et al*., 2017). The co-occurrence and temporal variability of the two species with comparatively low abundances of *T. quinqueloba* indicates surface waters between the Polar and Arctic Fronts (Johannessen *et al*., 1994; Kohfeld *et al.*, 1996; Pflaumann *et al.*, 1996, 2003; Eynaud *et al*., 2009; Husum and Hald, 2012). In addition, latitudinal displacement of the Arctic Front to the south and the presence of Arctic waters at the Site U1304 during both the glacial and interglacial periods can be assumed, particularly between 1.6–1.35 and 1.2–0.6 Ma (Figure 2).

Depth habitat differences between *N. pachyderma* and *T. quinqueloba*, and interspecies $\Delta\delta^{18}O$ facilitate reconstruction of the past stratification of the upper ocean (Mulitza *et al*., 1997; Chaisson and Ravelo, 2000; Sato *et al*., 2008). Simstich *et al.* (2003) inferred that the $\Delta\delta^{18}O_{Npachy\text{-}Tquin}$ indicates instability of the thermal stratification of surface waters, with higher $\Delta\delta^{18}O_{Npachy\text{-}Tquin}$ values indicating an input of stratified warmer Atlantic-sourced waters, whereas lower values may display surface waters originating from around the Polar Front and the East Greenland Current. In contrast, data from a sediment trap experiment in the Irminger Sea (Figure 1) show similar calcification depths of *N. pachyderma* and *T. quinqueloba* just below the surface mixed layer. Consequently, isotopic difference between these species may indicate phenology and changes in the past seasonality (Jonkers *et al*., 2010). Since production of *N. pachyderma* follows a bimodal pattern in spring and late summer (Tølderlund and Bé, 1971; Jonkers *et al*., 2010), and maximum production and flux of *T. quinqueloba* is unimodal during summer and autumn in the Irminger Sea, the isotopic differences between the species may rather display production of tests during different seasons than differences in water depths habitats (Jonkers *et al*., 2010, 2013). Also, in the GINS, *N. pachyderma* it is characterized by a single production period in summer (Kohfeld *et al*., 1996; Bauch *et al*., 1997; Volkmann and Mensch, 2001). Plankton tows from further south of our Site U1304 in the North Atlantic (Tølderlund and Bé, 1971) revealed a bimodal seasonal abundance pattern for *T. quinqueloba*. The relatively small $\Delta\delta^{18}O_{Npachy\text{-}Tquin}$ of 0.2 to 0.8‰ indicates cooler Arctic type surface waters at the Site U1304 during Phase I (Figure 3C), with the Arctic Front located to the south of the site. However, seasonal effects and the phenology of planktic foraminifers at the latitude of the Site U1304 may have been more similar to the Irminger Sea than the GINS, and the $\Delta\delta^{18}O_{Npachy\text{-}Tquin}$ may rather result from differences in the seasonal production than different water depths habitats.

Temporal absence of *N. pachyderma* from the planktic foraminiferal community over extended time-periods around 1.3 Ma (MIS 42–37) coincides with the presence of warm-water indicators, and deposition of diatomaceous oozes characterized by *T. longissima* (Shimada *et al*., 2008), implying a northward retreat of the Arctic waters. Unfortunately, sufficient numbers of *N. pachyderma* tests for stable isotope analyses could not be obtained from this time-interval, and the temporal resolution is too low to provide further paleoceanographic information here.

At the end of Phase I, relative abundances of *N. pachyderma* gradually decreased since 0.8 Ma (MIS 20), even though the faunal assemblages at the Site U1304 are still characterized by a dominance of *N. pachyderm*a (Figure 2). At the IODP Site U1305, at Erik Ridge, in the Labrador Sea, the surface hydrology had changed from more balanced open oceanic to more variable conditions at the regional scale just after *ca.* 0.8 Ma (MIS 20; Hillaire-Marcel *et al.*, 2011). The signal might be part of the Mid-Pleistocene Transition because glacial/interglacial $\delta^{18}O$

values range at 2.0–3.6‰ prior to *ca.* 0.8 Ma, while varying from 2.3 to 4.5‰ later in the record of Site U1305 (Hillaire-Marcel *et al.*, 2011). As Site U1304 is located far southeast of Site U1305 (Figure 1), gradual decrease of *N. pachyderma* from 0.8 Ma may indicate expanding surface waters from the Labrador Sea to the southeast.

Phase II, 0.6–0.4 Ma, MIS 15–11

Neogloboquadrina pachyderma remained the dominant element of the planktic foraminiferal assemblage in Phase II. Increasing abundances of *T. quinqueloba* at Site U1304, and at ODP Site 984 (Figure 1) about 1100 km northeast of U1304 (Wright and Flower, 2002), suggest that Atlantic waters had spread northward across Site U1304 and approaching the Site ODP 984 between 0.6 Ma and 0.4 Ma (MISs 15 to 11). This assumption is supported by the occurrence of ooze-forming warm water diatom species during 0.6–0.4 Ma interval (Shimada *et al*., 2008).

The most drastic benthic isotope excursion of the past 3.2 Ma coincides with an input of IRD at *ca.* 0.64 Ma (MIS16) from the Hudson Bay at the Site U1308 (Hodell *et al.*, 2008; Hodell and Channell, 2016), located southeast of the Site U1304 (Figure 1). These findings suggest that the late Pleistocene surface waters also at the Site U1304 may have been increasingly affected by southern sourced Atlantic waters. Although the exact timing of the isotope excursion at Termination VII, at Site U1308, is slightly different (possibly affected by differences in sampling resolution) from the developments at Site U1304, including changes in the abundance of *T. quinqueloba* at Site U1304, the Subarctic Front is assumed to have fully developed at Site U1304 at the transition between Phases I and II around 0.6 Ma. As a consequence, strengthening of the Subarctic Front is assumed to have accelerated intermittent diatom production and diatom ooze formation, whereas the Arctic Front may have merely displaced without any significant effect on the diatom production and sediment formation at Site U1304 (Shimada *et al.*, 2008). The $\Delta\delta^{18}O_{Npachy\text{-}Tquin}$ values are highly variable but still lower than in the following Phase III (Figure 3C), and indicate relatively cooler surface waters at Site U1304 still being bathed in Arctic waters during Phase II. Consequently, Phase II may be regarded as a transitional time-interval between Phases I and III.

Phase III, 0.4 Ma to Holocene; MIS 11–1

The boundary between Phases II and III is characterized by the most vigorous changes throughout the studied Site U1304 concerning the species assemblage of planktic foraminifers, temporal changes in test size and the morphology of *N. pachyderma* (Figure 2 and Appendix 1), and $\Delta\delta^{18}O_{Npachy\text{-}Tquin}$ (Figure 3). Since *ca.* 0.4 Ma (MIS 11), *N. pachyderma* abundances have been fluctuating at a higher amplitude than before, ranging from zero to 96.2% (Figure 2). The associated species, *G. bulloides*, *N. dutertrei*, and *G. scitula* were present at low to moderate abundances throughout Phase III. *Globigerina bulloides*, *G. scitula*, and *N. dutertrei* are typical elements of the transitional and subtropical ocean, and assumed to indicate an influence of the warmer Atlantic waters at the higher latitude Site U1304 (Johannessen *et al.*, 1994; Pflaumann *et al*., 1996; Husum and Hald, 2012). Occurrence of these species at a glacial/interglacial cyclicity also indicates that warmer Atlantic waters bathed the Site U1304 during the interglacials analogous to the modern hydrographic setting, and the Subarctic Front migrated to the south across the Site U1304 during the glacial/stadial periods (Ruddiman and Glover, 1975; Pflaumann *et al*., 1996). The Phases II to III boundary corresponds to the Mid-Brunhes Event, MBE (Droxler *et al*., 2003), which marks the onset of warmer interglacials over the late Quaternary, including the warm MIS 11 (Hodell *et al*., 2003; Voelker *et al*., 2010), and maximum amplitudes in $\delta^{18}O$ and mean global temperatures between glacial and interglaical stages (Lisiecki and Raymo, 2005). Pollen analyses at the ODP Site 646 provide data on the vegetation density and imply nearly ice-free episodes in southern Greenland during the warm interval of MIS 11 (de Vernal and Hillaire-Marcel, 2008).

Larger and more rounded *N. pachyderma* tests following the Phases II to III boundary (Figure 3D, E) at Site U1304 are similar to those from the northern North Atlantic >66°N (Huber *et al*., 2000). Tests of *N. pachyderma* have been shown to increase in size with decreasing sea surface temperature (Möller *et al*., 2013). Adaptation of *N. pachyderma* to specific cold-water conditions and the resulting changes in relative abundance have been applied to reconstruct periodical migrations of the Subarctic Front over glacial/interglacial cycles (MIS 5/6; Mokeddem and McManus, 2016), similar to Site U1304 just after the boundary between Phases II and III (Figure 2).

From the mid latitude to subtropical ocean, MIS 11 was warmer than the Holocene (Kandiano *et al*., 2012), and the Atlantic Meridional Ocean Circulation (AMOC) strengthened (Rodríguetz-Tovar *et al*., 2015; Doherty and Thibodeau, 2018). Numerical experiments suggest that the AMOC was amplified by anomalous wind stress curl that drives enhanced salt transport from the low- to high-latitude North Atlantic during MIS 11 (Rachmayani *et al*., 2017). In the GINS, surface water temperatures were low during MIS 11 (Helmke and Bauch, 2003; Kandiano and Bauch, 2007; Kandiano *et al*., 2012). In the western GINS, a thick and cold surface layer prevailed due to meltwater inflow (Thibodeau *et al*., 2017; Kandiano *et al*., 2016) originating from the Arctic Ocean (Doherty and

Thibodeau, 2018; Cronin *et al*., 2019), and from continuous melting of the Greenland Ice Sheet (Kandiano *et al*., 2017). The cold and fresh waters expanded to southeast around Site M23414 located to the east of Site U1304 (Kandiano and Bauch, 2007; Kandiano *et al*., 2017). Moreover, meltwaters from the Greenland Ice Sheet reached Eric Drift in the Labrador Sea during MIS 11 (Reyes *et al*., 2014). Due to eastward expansion of these cold and fresh surface waters from the Nordic Seas and Arctic Ocean, the axis of the North Atlantic Current displaced to the east, and caused moderate abundances of *N. pachyderma* during MIS 11 at Site U1304. Since the Holocene samples from Site U1304 yield only 4.6% of relative abundance of *N. pachyderma* on average (Appendix 1), it seems to be slightly colder during MIS 11 than Holocene at Site U1304. Following the MBE and MIS 11 until the Holocene, surface waters changed to a modern-type hydrology with enhanced seasonal contrasts in SST (Jonkers *et al*., 2010) indicated by $\Delta\delta^{18}O_{Npachy\text{-}Tquin}$ values (Figure 3C). The onset of the migration of surface waters at Site U1304 starting from MIS 11 may be linked to the establishment of post-Mid-Brunhes interglacial settings of Arctic Intermediate Water, surface productivity, and sea ice conditions at the Arctic Ocean (Cronin *et al*., 2017). Consequently, two-tiered migration of the North Atlantic waters both at the boundaries at Phases I/II and II/III, corresponding to MIS 15 (*ca.* 0.6 Ma) and MIS 11 (*ca.* 0.4 Ma), respectively, are demonstrated by the multi proxy data at the Site U1304.

Trophic effects on planktic foraminifer test size

Small average test sizes of *N. pachyderma* at the boundaries between Phases I and II during MIS 15, and Phases II and III during MIS 11 at Site U1304 (Figure 3D) are assumed to indicate improved trophic conditions during time-intervals of environmental turnover, reorganization of hydrologic fronts, and enhanced availability of nutrients for primary production in the surface ocean. As an R-selected species, *N. pachyderma* follows an opportunistic feeding strategy, and early reproduction during the ontogenetic development, i.e., as young adults with relatively small tests (Schiebel *et al*., 2017; Schiebel and Hemleben, 2017). Thick diatomaceous oozes deposited during MIS 11 show the persistent location of the Subarctic Front around Site U1304, enhanced supply of nutrients to the surface ocean, and enhanced primary production (Shimada *et al.*, 2008; Xuan *et al.*, 2016). This finding supports the observation that smaller-sized species and specimens occur in areas affected by hydrologic fronts (Schmidt *et al*., 2004). Consequently, the test-size development of *N. pachyderma* over the past 1.6 Ma at the IODP Site U1304 may result from changing trophic conditions, resulting from changing hydrologic conditions such as upwelling, and an enhanced availability of diatoms (i.e., prey production) along the Subarctic Front (Shimada *et al*., 2008).

Conclusions

Temporal analyses of assemblages, stable oxygen isotope, and test morphometry of planktic foraminifera of the IODP Site U1304 over the past 1.6 million years suggest a two-tiered geographic migration of the North Atlantic waters and associated fronts.

Superimposed on an evolutionary long-term test size increase of the planktic foraminiferal species *Neogloboquadrina pachyderma* over 1.6 Ma, larger and smaller tests have been produced during glacial and interglacial conditions, respectively. Following a major step in evolutionary test-size adaptation around 1.1–1.0 Ma, modern-type test-sizes were reached by 0.6 Ma in MIS 15. Our findings suggest that the test size of *N. pachyderma* at the Site U1304 has been affected by the meridional migration of the Subarctic Front over the past 0.4 Ma. More elongated specimens of *N. pachyderma* appeared with a sudden decrease in test size during the MIS 11. We infer that the test morphology of *N. pachyderma* documents adaptation under the hydrologic conditions in the nutrient-rich frontal zone over the long-lasting interglacial MIS 11.

Predominance of *N. pachyderma*, reflecting the cold waters originating from polar regions, has been recognized almost throughout the entire studied section, except for a short time-interval around 1.3 Ma, suggesting persistence of Arctic waters throughout glacial/interglacial time-intervals in Phase I (1.6–0.6 Ma).

Following Termination VII at the MISs 16/15 boundary, the Subarctic Front episodically approached the Site U1304 during the interglacial periods, while mostly Arctic waters bathed the region. In Phase II, from 0.6 to 0.4 Ma, *N. pachyderma* remained the dominant element of the planktic foraminiferal assemblage in association with enhanced numbers of *T. quinqueloba* in the interglacials. Phase II may be regarded as a transitional time-interval from Phases I to III.

Phase III, from *ca.* 0.4 Ma (MIS 11), has been characterized by high $\Delta\delta^{18}O_{Npachy\text{-}Tquin}$ values, larger *N. pachyderma* test sizes, and high amplitude changes in the relative abundance of *N. pachyderma* associated with warmer water species *G. bulloides*, *G. scitula*, and *N. dutertrei*. These changes indicate the presence of warm Atlantic waters at Site U1304. In Phase III, the presence of monospecific diatom oozes indicates a major advance and retreat of the Subarctic Front across the Site U1304 (Shimada *et al.*, 2008).

Our multiproxy analyses of planktic foraminifera suggest establishment of the modern oceanographic condition

by a two-tiered change of the oceanic waters and fronts at *ca.* 0.6 Ma (MIS 15) and 0.4 Ma (MIS 11). Our study also shows that multiproxy analyses of low-diversity planktic foraminiferal assemblages in subpolar to polar regions facilitate detailed reconstruction of paleoceanography and paleoclimate.

Acknowledgements

We sincerely appreciate the support of captain, crew, and technical staff of the IODP Expedition 303. Special thanks also to Mari Matsui and Akiko Osaki for the faunal sample preparations, Michiyo Kobayashi and Sayaka Sakaguchi for the isotopic analysis at CMCR, Kochi University, and Aurore Movellan for help with the morphological analysis at the Université d'Angers, France. Yuichiro Tanaka (AIST) gave valuable comments and encouragements. We gratefully acknowledge the highly valuable comments of two anonymous reviewers. Financial support was given by the Japan Society for the Promotion of Science to MY (Grant-in-Aid for Scientific Research; KAKENHI, nos. 21740361 and 24740346). Also, this study was performed under the cooperative research program of CMCR, Kochi University (accept nos. 09B039 and 10B043).

References

Alonso-Garcia, M., Sierro, F. J. and Flores, J. A., 2011: Arctic front shifts in the subpolar North Atlantic during the Mid-Pleistocene (800–400 ka) and their implications for ocean circulation. *Palaeogeography*, *Palaeoclimatology*, *Palaeoecology*, vol. 311, p. 268–280.

Andersen, C., Koç, N. and Moros, M., 2004: A highly unstable Holocene climate in the subpolar North Atlantic: evidence from diatoms. *Quaternary Science Reviews*, vol. 23, p. 2155–2166.

Barker, S., Chen, J., Gong, X., Jonkers, L., Knorr, G. and Thornalley, D., 2015: Icebergs not the trigger for North Atlantic cold events. *Nature*, vol. 520, p. 333–336.

Bauch, D., Carstens, J. and Wefer, G., 1997: Oxygen isotope composition of living *Neogloboquadrina pachyderma* (sin.) in the Arctic Ocean. *Earth and Planetary Science Letters*, vol. 147, p. 47–58.

Bé, A. W. H., 1960: Ecology of recent planktonic foraminifera—Part 2, Bathymetric and seasonal distributions in the Sargasso Sea off Bermuda. *Micropaleontology*, vol. 6, p. 373–392.

Bé, A. W. H. and Tølderlund, D. S., 1971: Distribution and ecology of living planktonic foraminifera in surface waters of the Atlantic and Indian Oceans. *In*, Funnel, B. M. and Riedel, W. R. *eds.*, *The Micropalaeontology of Oceans*, p. 105–149. Cambridge University Press, Cambridge.

Bodén, P. and Backman, J., 1996: A laminated sediment sequence from the northern North Atlantic Ocean and its climatic record. *Geology*, vol. 24, p. 507–510.

Carstens, J., Hebbeln, D. and Wefer, G., 1997: Distribution of planktic foraminifera at the ice margin in the Arctic (Fram Strait*). Marine Micropaleontology*, vol. 29, p. 257–269.

Chaisson, W. P. and Ravelo, A. C., 2000: Pliocene development of the east-west hydrographic gradient in the equatorial Pacific. *Paleoceanography*, vol. 15, p. 497–505.

Channell, J. E. T., Sato, T., Kanamatsu, T., Stein, R., Malone, M. J., Alvarez-Zarikian, C. A. and the IODP Expedition 303/306 Scientists, 2006: IODP Expeditions 303 and 306 Monitor Miocene-Quaternary Climate in the North Atlantic. *Scientific Drilling*, doi:10.2204/iodp.sd.2.01.2006.

Crocket, K. C., Vance, D., Gutjahr, M., Foster, G. L. and Richards, D. A., 2011: Persistent Nordic deep-water overflow to the glacial North Atlantic. *Geology*, vol. 39, p. 515–518.

Cronin, T. M., Dwyer, G. S., Caverly, E. K., Farmer, J., DeNinno, L. H., Rodriguez-Lazaro, J. and Gemery, L., 2017: Enhanced Arctic amplification began at the Mid-Brunhes Event ~400,000 years ago. *Scientific Reports*, doi: 10.1038/s41598-017-13821-2.

Cronin, T. M., Keller, K. J., Farmer, J. R., Schaller, M. F., O'Regan, M., Poirier, R., Coxall, H., Dwyer, G. S., Bauch, H., Kindstedt, I. G., Jakobsson, M., Marzen, R. and Santin, E., 2019: Interglacial paleoclimate in the Arctic. *Paleocenography and Paleoclimatology*, vol. 34, p. 1959–1979.

Darling, K., Kucera, M., Kroon, D. and Wade, C. M., 2006: A resolution for the coiling direction paradox in *Neogloboquadrina pachyderma*. *Paleoceanography*, doi: 10.1029/2005PA001189.

de Vernal, A. and Hillaire-Marcel, C., 2008: Natural variability of Greenland climate, vegetation and ice volume during the last million years. *Science*, vol. 320, p. 1622–1625.

Doherty, J. M. and Thibodeau, B., 2018: Cold water in a warm world: Investigating the origin of the Nordic Seas' surface properties during MIS 11. *Frontiers in Marine Science*, vol. 5, p. 1–11.

Droxler, A. W., Alley, R. B., Howard, W. R., Poore, R. Z. and Burckle, L. H., 2003: Unique and exceptionally long interglacial marine isotope stage 11: window into earth warm future climate. *In*, Droxler, A. D., Poore, R. Z. and Burckle, L. H. *eds.*, *Earth's climate and orbital eccentricity, the Marine Isotope Stage 11 Question*, p. 1–14. Geophysical Monograph Series, vol. 137, Blackwell Publishing, London.

Duplessy, J. C., Shackleton, N. J., Fairbanks, R. G., Labeyrie, Oppo, D. and Kallel, N., 1988: Deepwater source variations during the last climate cycle and their impact on the global deepwater circulation. *Paleoceanography*, vol. 3, p. 343–360.

Eldevik, T., Straneo, F., Sandø, A. B. and Furevik, T., 2005: Pathways and export of Greenland Sea water. *In*, Drange, H., Dokken, T., Furevik, T., Gerdes, R. and Berger, W. *eds*., *The Nordic Seas: an integrated perspective*, p. 89–103, American Geophysical Union, Washington, DC.

Expedition 303 Scientists, 2006: Site U1304. *In*, Channell, J. E. T., Kanamatsu, T., Sato, T., Stein, R., Alvarez Zarikian, C. A., Malone, M. J. *eds.*, *Proceedings of the Integrated Ocean Drilling Program, volume 303/306 Expedition Reports*. doi: 10.2204/iodp.proc.303306.104.2006. Integrated Ocean Drilling Program Management International, Inc., College Station.

Eynaud, F. E., Cronin, T. M., Smith, S. A., Zaragosi, S., Mavel, J., Mary, Y., Mas, V. and Pujol, C., 2009: Morphological variability of the planktonic foraminifer *Neogloboquadrina pachyderma* from ACEX cores: Implications for Late Pleistocene circulation in the Arctic Ocean. *Micropaleontology*, vol. 55, p. 101–116.

Fogelqvist, E., Blindheim, J., Tanhua, T., Østerhus, S., Buch, E. and Rey, F., 2003: Greenland-Scotland overflow studied by hydrochemical multivariate analysis. *Deep-Sea Research I*, vol. 50, p. 73–102.

Gordon, A. L., 1982: Weddell deep water variability. *Journal of Marine Research*, vol. 40, p. 199–217.

Hald, M., 2001: Climate change and paleoceanography. *In*, Schäfer, P., Ritzrau, W., Schlüter, M. and Thiede, J. *eds*. *The Northern North Atlantic: A Changing Environment*, p. 281–290, Springer, Berlin.

Hayashi, T. and Ono, M., 2019: Diatoms in Upper Pliocene–Lower Pleistocene sediments, subpolar North Atlantic: 1. *Thalassiothrix Antarctica*. *Diatom*, vol. 35, p. 18–27.

Helmke, J. P. and Bauch, H. A., 2003: Comparison of glacial and interglacial conditions between the polar and subpolar North Atlantic region over the last five climatic cycles. *Paleoceanography*, doi: 10.1029/2002PA000794.

Hillaire-Marcel, C. and Bilodeau, G., 2000: Instabilities in the Labrador Sea water mass structure during the last climatic cycle. *Canadian Journal of Earth Sciences*, vol. 37, p. 795–809.

Hillaire-Marcel, C. and de Vernal, A., 2008: Stable isotope clue to episodic sea ice formation in the glacial North Atlantic. *Earth and Planetary Science Letters*, vol. 268, p. 143–150.

Hillaire-Marcel, C., de Vernal, A., Bilodeau, G. and Weaver, A. J., 2001: Absence of deep-water formation in the Labrador Sea during the last interglacial period. *Nature*, vol. 410, p. 1073–1077.

Hillaire-Marcel, C., de Vernal, A. and McKay, J., 2011: Foraminifer isotope study of the Pleistocene Labrador Sea, northwest North Atlantic (IODP Sites 1302/03 and 1305), with emphasis on paleoceanographical differences between its "inner" and "outer" basins. *Marine Geology*, vol. 279, p. 188–198.

Hillaire-Marcel, C., de Vernal, A., Polyak, L. and Darby, D., 2004: Size-dependent isotopic composition of planktic foraminifers from Chukchi Sea vs. NW Atlantic sediments—implications for the Holocene paleoceanography of the western Arctic. *Quaternary Science Reviews*, vol. 23, p. 245–260.

Hodell, D. A. and Channell, J. E. T., 2016: Mode transitions in Northern Hemisphere glaciation: co-evolution of millennial and orbital variability in Quaternary climate. *Climate of the Past*, vol. 12, p. 1805–1828.

Hodell, D. A., Channell, J. E. T., Curtis, J. H., Romero, O. E. and Röhl, U., 2008: Onset of "Hudson Strait" Heinrich events in the eastern North Atlantic at the end of the middle Pleistocene transition (~640 ka)? *Paleoceanography*, doi: 10.1029/2008PA001591.

Hodell, D. A., Kanfoush, S. L., Venz, K. A., Charles, C. D. and Sierro, F. J., 2003: The Mid-Brunhes transition in ODP Sites 1089 and 1090 (Subantarctic South Atlantic). *In*, Droxler, A. D., Poore, R. Z. and Burckle, L. H. *eds.*, *Erath's climate and orbital eccentricity, the Marine Isotope Stage 11 Question*, p. 113–129. Geophysical Monograph Series, vol. 137, Blackwell Publishing, London.

Hodell, D. A., Minth, E. K., Curtis, J. H., McCave, I. N., Hall, I. R., Channell, J. E. T. and Xuan, C., 2009: Surface and deep-water hydrography on Gardar Drift (Iceland Basin) during the last interglacial period. *Earth and Planetary Science Letters*, vol. 288, p. 10–19.

Howe, J. N. W., Piotrowski, A. M., Noble, T. L., Mulitza, S., Chiessi, C. M. and Bayon, G., 2016: North Atlantic deep water production during the Last Glacial Maximum. *Nature Communications*, doi: 10.1038/ncomms11765.

Huber, R., Meggers, H., Baumann, K.-H., Raymo, M. E. and Heinrich, R., 2000: Shell size variation of the planktonic foraminifer *Neogloboquadrina pachyderma* sin. in the Norwegian-Greenland Sea during the last 1.3 Myrs: implications for paleoceanographic reconstructions. *Palaeogeography*, *Palaeoclimatology*, *Palaeoecology*, vol. 160, p. 183–212.

Husum, K. and Hald, M., 2012: Arctic planktic foraminiferal assemblages: Implications for subsurface temperature reconstructions. *Marine Micropaleontology*, vols. 96 and 97, p. 38–47.

Johannessen, T., Jansen, E., Flatøy, A. and Ravelo, A. C., 1994: The relationship between surface water masses, oceanographic fronts and paleoclimatic proxies in surface sediments of Greenland, Iceland, Norwegian Seas. *In*, Zahn, R., Pedersen, T. F., Kaminski, M. A. and Labeyrie, L. *eds*., *Carbon Cycling in the Glacial Ocean: Constraints on the Ocean's Role in Global Change*, p. 61–85. NATO ASI Series book series, vol. 17, Springer, Belrin and Heidelberg.

Jonkers, L., Brummer, G.-J. A., Peeters, F. J. C., van Aken, H. M. and DeJong, M. F., 2010: Seasonal stratification, shell flux, and oxygen isotope dynamics of left-coiling *N. pachyderma* and *T. quinqueloba* in the western subpolar North Atlantic. *Paleoceanography*, doi: 10.1029/2009PA001849.

Jonkers, L., van Heuven, S., Zahn, R. and Peeters, F. J. C., 2013: Seasonal patterns of shell flux, $\delta^{18}O$ and $\delta^{13}C$ of small and large *N. pachyderma* (s) and *G. bulloides* in the subpolar North Atlantic. *Paleoceanography*, doi: 10.1002/palo.20018.

Kandiano, E. S. and Bauch, H. A., 2007: Phase relationship and surface water mass change in the northeast Atlantic during marine isotope stage 11 (MIS 11). *Quaternary Research*, doi: 10.1016/j.yqres.2007.07.009.

Kandiano, E. S., Bauch, H. A., Fahl, K., Helmke, J. P., Röhl, U., Pérez-Folgado, M. and Cacho, I., 2012: The meridional temperature gradient in the eastern North Atlantic during MIS 11 and its link to the ocean-atmosphere system. *Palaeogeography*, *Palaeoclimatology*, *Palaeoecology*, vol. 333–334, p. 24–39.

Kandiano, E. S., van der Meer, M. T. J., Bauch, H. A., Helmke, J., Damsté, J. S. S. and Schouten, S., 2016: A cold and fresh ocean surface in the Nordic Seas during MIS 11: Significance for the future ocean. *Geophysical Research Letters*, vol. 43, p. 10929–10937.

Kandiano, E. S., van der Meer, M. T. J., Schouten, S., Fahl, K., Sinninghe Damsté, J. S. and Bauch, H. A., 2017: Response of the North Atlantic surface and intermediate ocean structure to climate warming of MIS 11. *Scientific Reports*, doi:10.1038/srep46192.

Kennett, J. P. and Srinivasan, M. S., 1980: Surface ultrastructural variation in *Neogloboquadrina pachyderma* (Ehrenberg): phenotype variation and phylogeny in the Late Cenozoic. *Cushman Foundation Special Publication*, no. 19, p. 134–162.

Kohfeld, K. E., Fairbanks, R. G., Smith, D. L. and Walsh, I. D., 1996: *Neogloboquadrina pachyderma* (sinistral coiling) as paleoceanographic tracers in polar oceans: Evidence from Northeast Water Polynya plankton tows, sediment traps, and surface sediments. *Paleoceanography*, vol. 11, p. 679–699.

Kucera, M. and Kennett, J. P., 2002: Causes and consequences of a middle Pleistocene origin of the modern planktonic foraminifer *Neogloboquadrina pachyderma* sinistral. *Geology*, vol. 30, p. 539–542.

Lisiecki, L. E. and Raymo, M. E., 2005: A Pliocene-Pleistocene stack of 57 globally distributed benthic $\delta^{18}O$ records. *Paleoceanography*, doi:10.1029/2004PA001071.

Marshall, J. and Schott, F., 1999: Open-ocean convection: observations, theory, and models. *Reviews of Geophysics*, vol. 37, p. 1–64.

Matsumoto, K., 2017: Tantalizing evidence for the glacial North Atlantic bottom water. *Proceedings of the National Academy of Sciences of the United States of America*, vol. 114, p. 2794–2796.

McManus, J. F., Bond, G. C., Broecker, W. S., Johnsen, S., Labeyrie, L. and Higgins, S., 1994: High-resolution climate records from the North Atlantic during the last interglacial. *Nature*, vol. 371, p. 326–329.

Meincke, J., 2002: Climate dynamics of the North Atlantic and NW-Europe: An observation-based overview. *In*, Wefer, G., Berger, W., Behre, K.-E. and Jansen, E. *eds*., *Climate Development and History of the North Atlantic Realm*, p. 25–40. Springer-Verlag, Berlin.

Mokeddem, Z. and McManus, F., 2016: Persistent climatic and oceanographic oscillations in the subpolar North Atlantic during the MIS 6 glaciation and MIS 5 interglacial. *Paleoceanography*, vol. 31,

p. 758–778.
Möller, T., Schulz, H. and Kucera, M., 2013: The effect of sea surface properties on shell morphology and size of the planktonic foraminifer *Neogloboquadrina pachyderma* in the North Atlantic. *Palaeogeography*, *Palaeoclimatology*, *Palaeoecology*, vol. 391, p. 34–48.
Mulitza, S., Niebler, H. S., Dürkoop, A., Hale, W. and Wefer, G., 1997: Planktonic foraminifera as recorders of past surface-water stratification. *Geology*, vol. 25, p. 335–338.
Oppo, D. W. and Lehman, S. J., 1995: Suborbital timescale variability of North Atlantic Deep Water during the past 200,000 years. *Paleoceanography*, vol. 10, p. 901–910.
Oppo, D. W., McManus, J. F. and Cullen, J. L., 2006: Evolution and demise of the last interglacial warmth in the subpolar North Atlantic. *Quaternary Science Reviews*, vol. 25, p. 3268–3277.
Pados, T. and Spielhagen, R. F., 2014: Species distribution and depth habitat of recent planktic Foraminifera in Fram Strait, Arctic Ocean. *Polar Research*, doi: 10.3402/polar.v33.22483.
Pflaumann, U., Duprat, J., Pujol, C. and Labeyrie, L., 1996: SIMMAX: a modern analog technique to deduce Atlantic sea surface temperatures from planktonic foraminifera in deep-sea sediments. *Paleoceanography*, vol. 11, p. 15–35.
Pflaumann, U., Sarnthein, M., Chapman, M., d'Abreu, L., Funnell, B., Duprat, M., Huels, M., Kiefer, T., Maslin, M., Schultz, H., Swallow, J., van Kreveld, S., Vautravers, M., Vogelsang, E. and Weinelt, M., 2003: Global North Atlantic: sea-surface conditions reconstructed by GLAMAP 2000. *Paleoceanography*, doi: 10.1029/2002PA000774.
Rachmayani, R., Prange, M., Lunt, D. J., Stone, E. J. and Schulz, M., 2017: Sensitivity of the Greenland Ice Sheet to interglacial climate forcing: MIS 5e versus MIS 11. *Paleoceanography*, doi: 10.1002/2017PA003149.
Repschläger, J., Weinelt, M., Andersen, N., Garbe-Schönberg, D. and Schneider, R., 2015: Northern source for Deglacial and Holocene deepwater composition changes in the Eastern North Atlantic Basin. *Earth and Planetary Science Letters*, vol. 425, p. 256–267.
Reyes, A. V., Carlson, A. E., Beard, B. L., Hatfield, R. G., Stoner, J. S., Winsor, K., Welke, B. and Ullman, D. J., 2014: South Greenland ice-sheet collapse during Marine Isotope Stage 11. *Nature*, vol. 510, p. 525–528.
Risebrobakken, B., Dokken, T. and Jansen, E., 2005: Extent and variability of the meridional Atlantic circulation in the eastern Nordic Seas during Marine Isotope Stage 5 and its influence on the inception of the Last Glacial. *In*, Drange, H., Dokken, T., Furevik, T., Gerdes, R. and Berger, W. *eds*., *The Nordic Seas: an integrated perspective*, p. 323–339. American Geophysical Union, Washington, DC.
Rodríguez-Tovar, F. J., Dorador, J., Martin-Garcia, G. M., Sierro, F. J., Flores, J. A. and Hodell, D. A., 2015: Response of macrobenthic and foraminifer communities to changes in deep-sea environmental conditions from marine isotope stage (MIS) 12 to 11 at the "Shackleton Site." *Global and Planetary Change*, vol. 133, p. 176–187.
Ruddiman, W. F. and Glover, L. K., 1975: Subpolar North Atlantic circulation at 9300 yr BP: faunal evidence. *Quaternary Research*, vol. 5, p. 361–389.
Sato, K., Oda, M., Chiyonobu, S., Kimoto, K., Domitsu, H. and Ingle Jr., J. C., 2008: Establishment of the western Pacific warm pool during the Pliocene: Evidence from planktic foraminifera, oxygen isotopes, and Mg/Ca ratios. *Palaeogeography*, *Palaeoclimatology*, *Palaeoecology*, vol. 265, p. 140–147.
Schiebel, R. and Hemleben, C., 2017: *Planktic foraminifers in the modern ocean*, 358 p. Springer-Verlag, Berlin and Heidelberg.
Schiebel, R. and Movellan, A., 2012: First-order estimate of the planktic foraminifer biomass in the modern ocean. *Earth System Science Data*, vol. 4, p. 75–89.
Schiebel, R., Spielhagen, R. F., Garnier, J., Hagemann, J., Howa, H., Jentzen, A., Martínez-Garcia, A., Meilland, J., Michel, E., Repschläger, J., Salter, I., Yamasaki, M. and Haug, G., 2017: Modern planktic foraminifers in the high-latitude ocean. *Marine Micropaleontology*, vol. 136, p. 1–13.
Schmidt, D. N., Renaud, S. and Bollmann, J., 2003: Response of planktic foraminiferal size to late Quaternary climate change. *Paleoceanography*, doi: 10.1029/2002PA000831.
Schmidt, D. N., Renaud, S., Bollmann, J., Schiebel, R. and Thierstein, H. R., 2004: Size distribution of Holocene planktic foraminifer assemblages: biogeography, ecology and adaptation. *Marine Micropaleontology*, vol. 50, p. 319–338.
Schröder-Ritzrau, A., Andruleit, H., Jensen, S., Samtleben, C., Schäfer, P., Matthiessen, J., Hass, H. C., Kohly, A. and Thiede, J., 2001: Distribution, export and alteration of fossilizable plankton in the Nordic Seas. *In*, Schäfer, P., Ritzrau, W., Schlüter, M. and Thiede, J. *eds*., *The Northern North Atlantic: A Changing Environment*, p. 81–104. Springer, Berlin.
Shimada, C., Sato, T., Toyoshima, S., Yamasaki, M. and Tanimura, Y., 2008: Paleoecological significance of laminated diatomaceous oozes during the middle-to-late Pleistocene, North Atlantic Ocean (IODP Site U1304). *Marine Micropaleontology*, vol. 69, p. 139–150.
Simstich, J., Sarnthein, M. and Erlenkeuser, H., 2003: Paired $\delta^{18}O$ signals of *Neogloboquadrina pachyderma* (s) and *Turborotalita quinqueloba* show thermal stratification structure in Nordic Seas. *Marine Micropaleontology*, vol. 48, p. 107–125.
Spielhagen, R. F., Werner, K., Sorensen, S. A., Zamelczyk, K., Kandiano, E., Budeus, G., Husum, K., Marchitto, T. M. and Hald, M., 2011: Enhanced modern heat transfer to the Arctic by warm Atlantic water. *Science*, vol. 331, p. 450–453.
Swift, J., 1986: The Arctic waters. *In*, Hurdle, B. *ed*., *The Nordic Seas*, p. 129–154. Springer, New York.
Thibodeau, B., Bauch, H. A. and Pedersen, T. F., 2017: Stratification induced variations in nutrient utilization in the Polar North Atlantic during past interglacials. *Earth and Planetary Science Letters*, vol. 457, p. 127–135.
Tølderlund, D. S. and Bé, A. W. H., 1971: Seasonal distribution of planktonic foraminifera in the western North Atlantic. *Micropaleontology*, vol. 17, p. 297–329.
Voelker, A. H. L., Rodrigues, T., Billups, K., Oppo, D., McManus, J., Stein, R., Hefter, J. and Grimalt, J. O., 2010: Variations in mid-latitude North Atlantic surface water properties during the mid-Brunhes (MIS 9—14) and their implications for the thermohaline circulation. *Climate of the Past*, vol. 6, p. 531–552.
Volkmann, R., 2000: Planktic foraminifers in the outer Laptev Sea and the Fram Strait—modern distribution and ecology. *Journal of Foraminiferal Research*, vol. 30, p. 157–176.
Volkmann, R. and Mensch, M., 2001: Stable isotope composition ($\delta^{18}O$, $\delta^{13}C$) of living planktic foraminifers in the outer Laptev Sea and the Fram Strait. *Marine Micropaleontology*, doi.org/10.1016/S0377-8398(01)00018-4.
Wright, A. K. and Flower, B. P., 2002: Surface and deep ocean circulation in the subpolar North Atlantic during the mid-Pleistocene revolution. *Paleoceanography*, doi: 10.1029/2002PA000782.
Xuan, C., Channell, J. E. T. and Hodell, D. A., 2016: Quaternary paleomagnetic and oxygen isotope records from diatom-rich sediments from the southern Gardar Drift (IODP Site U1304, North Atlantic), *Quaternary Science Reviews*, vol. 142, p. 74–89.
Yamasaki, M., Matsui, M., Shimada, C., Chiyonobu, S. and Sato, T.,

2008: Timing of shell size increase and decrease of the planktic foraminifer *Neogloboquadrina pachyderma* (sinistral) during the Pleistocene, IODP Exp. 303 Site U1304, the North Atlantic Ocean. *Open Paleontology Journal*, vol. 1, p. 18–23.

Author contributions

M. Y., M. I., and R. S. examined the materials by faunal and geochemical methods, and C. S. was responsible for the floral paleoecology. All authors participated in the discussion on Pleistocene microecology and paleoceanography, and writing of the manuscript.

Appendix 1. Relative abundance (%) of major foraminifera species.

	No.	1	2	3	4	5	6	7	8		No.	1	2	3	4	5	6	7	8
Core depth (mcd)	Age (Ka) by Xuan *et al.* (2016)	*Globigerina bulloides*	*Turborotalita quinqueloba*	*Globigerinita glutinata*	*Globorotalia inflata*	*Globorotalia scitula*	*Neogloboquadrina pachyderma*	*Neogloboquadrina incompta*	*Neogloboquadrina dutertrei*	Core depth (mcd)	Age (Ka) by Xuan *et al.* (2016)	*Globigerina bulloides*	*Turborotalita quinqueloba*	*Globigerinita glutinata*	*Globorotalia inflata*	*Globorotalia scitula*	*Neogloboquadrina pachyderma*	*Neogloboquadrina incompta*	*Neogloboquadrina dutertrei*
0.17	0.47	35.1	19.5	18.0	2.0	0.5	3.4	16.6	0	25.24	186.18	2.8	2.4	0	0	0	91.3	2.1	0
1.67	5.84	25.5	35.1	13.0	2.9	0	5.3	15.4	1.4	26.24	194.05	15.3	34.9	2.8	11.6	2.8	7.0	22.8	0.5
2.17	8.09	20.8	34.2	5.0	5.4	0	5.0	19.8	0	26.86	198.00	5.9	30.5	4.3	2.3	9.0	44.1	1.6	1.6
3.17	12.59	19.3	25.3	7.3	9.4	0	10.7	21.5	3.4	27.36	201.19	9.1	33.5	2.9	2.5	12.8	31.0	2.9	3.7
3.87	15.64	8.7	22.7	5.8	3.4	0	48.8	7.2	0	28.86	208.29	6.0	56.5	2.5	4.5	7.0	7.5	2.5	0
4.17	16.85	12.8	21.8	4.3	4.3	0	36.3	14.5	0	29.36	210.29	3.2	67.7	5.0	2.7	9.1	4.1	6.4	1.8
4.82	25.12	4.7	17.4	0	0	0	74.6	2.3	0	30.86	216.26	22.4	31.8	5.5	7.0	0.5	11.4	17.9	0
6.37	44.63	30.5	25.1	6.5	0.7	0.4	15.3	13.8	0	33.36	235.61	18.5	42.5	8.2	6.9	8.6	3.0	6.9	1.7
7.37	52.16	34.6	32.7	9.8	0	0	9.3	10.3	0.5	33.86	237.96	9.9	33.6	11.9	9.9	2.8	5.1	21.7	0
8.37	59.51	24.1	26.1	5.3	1.2	1.2	33.5	6.9	0	34.16	239.37	19.1	37.7	8.1	9.7	7.2	4.2	7.6	2.1
9.37	68.44	5.6	37.5	8.0	13.1	1.6	1.2	18.3	9.6	36.66	262.32	3.9	46.1	6.9	2.0	1.5	23.5	8.8	3.9
10.19	74.73	23.9	25.4	12.7	24.9	3.9	2.4	4.4	2.0	38.16	276.43	0	0	0	0	0	96.2	3.3	0
10.69	78.54	3.9	4.8	0.9	0	0	84.3	2.2	0	38.87	281.32	14.9	27.9	10.4	1.8	4.1	33.3	4.5	2.7
11.19	81.98	18.7	9.3	1.4	0	0	65.0	0.5	4.7	40.37	291.09	20.2	22.5	2.8	0.5	6.1	32.4	12.7	0
12.69	92.02	1.2	0.4	0	0	0	95.0	2.7	0	41.87	301.13	30.4	32.7	3.9	8.9	6.2	2.7	15.2	0
14.19	102.76	13.8	21.9	3.6	0	0.8	54.3	2.4	1.6	42.37	303.37	10.1	8.7	7.2	9.2	1.4	28.0	34.8	0
15.19	108.72	41.4	18.6	11.0	11.9	1.0	9.0	1.4	1.4	43.30	306.77	5.5	36.4	3.2	0.9	1.8	34.5	15.5	2.3
15.69	110.12	34.1	13.6	19.1	8.2	0.5	11.8	10.0	0	44.30	309.81	14.2	50.9	3.3	6.1	3.3	0.9	12.7	4.7
16.69	112.42	12.7	41.5	16.1	1.0	0	18.5	4.4	0	45.80	314.39	20.3	38.4	2.5	1.8	2.9	1.8	26.4	3.3
17.69	114.68	9.6	40.8	24.3	14.2	1.4	0.5	5.5	1.4	46.30	315.91	16.5	45.0	0	3.0	4.0	3.0	23.5	0
18.69	116.94	21.5	28.8	26.5	5.0	0.5	0.5	6.4	7.3	47.30	318.96	20.8	37.6	8.6	1.6	2.0	2.9	24.5	0.8
19.69	119.20	18.3	29.3	17.5	3.7	0	0	29.7	0.8	48.80	323.53	37.2	31.4	6.6	1.8	0	2.7	15.0	2.7
21.19	122.23	16.6	30.9	10.1	1.8	0.5	2.8	34.6	0	49.43	325.46	30.5	11.4	15.7	2.4	4.8	2.9	30.5	1.9
22.19	125.02	28.5	32.2	7.0	5.1	0	1.4	19.2	3.3	50.43	328.50	18.7	25.4	4.3	1.3	6.4	3.3	33.8	0
23.24	146.36	2.3	4.2	0	0	0	85.0	0	0	51.43	331.55	13.0	27.4	10.6	10.1	5.3	5.3	24.0	1.0
23.74	156.31	0.5	20.2	0.5	0	0	76.4	2.0	0	52.43	344.75	0.4	3.5	0.4	0	0	88.5	6.6	0

Appendix 1. *Continued.*

	No.	1	2	3	4	5	6	7	8		No.	1	2	3	4	5	6	7	8
53.43	362.65	1.4	51.9	1.0	0	1.0	42.3	1.9	0	101.68	536.37	1.6	24.8	0	0	0	65.4	6.9	0
54.26	374.98	14.0	40.2	1.4	3.3	1.9	28.0	7.9	0	102.67	543.23	0.0	27.7	0.4	0	0	69.8	1.8	0
54.76	376.49	0	12.1	0	0	0	84.0	2.9	0	103.67	550.17	0.5	13.5	0	0	0	83.7	1.9	0
55.76	379.51	5.4	46.5	0	1.2	0	36.8	8.1	1.2	104.87	555.54	4.0	42.0	0	1.2	0.8	43.2	5.6	0
56.76	382.53	10.5	55.0	1.9	4.3	1.9	8.1	15.8	1.0	105.37	557.33	11.5	24.8	1.8	16.1	0	39.9	3.2	0.5
58.26	387.05	7.4	31.1	0	1.6	0.8	48.0	8.6	0.8	105.87	559.12	2.4	31.4	2.4	1.9	0	57.5	3.9	0
58.76	388.56	13.4	21.6	9.3	8.2	4.1	10.4	29.4	0.4	108.86	569.81	16.1	26.5	2.8	6.6	2.4	19.0	22.7	0
59.26	390.07	11.7	39.8	6.8	4.4	1.5	6.3	29.1	0	109.86	573.39	18.1	34.1	4.7	14.7	2.2	15.1	9.5	0
59.87	391.90	4.1	5.4	0	1.4	0	84.7	4.5	0	110.36	575.18	3.7	31.3	2.1	7.0	0	46.1	7.4	0
60.87	394.54	4.9	40.2	2.0	2.9	0	27.0	20.1	2.5	110.86	576.97	11.1	44.9	0	7.8	0.4	17.3	16.5	0
61.37	395.86	16.9	12.3	5.6	5.6	0	27.5	30.4	0	111.87	581.64	1.0	25.2	1.9	0.5	0	65.5	5.8	0
62.37	398.50	4.2	18.1	4.2	4.7	0.9	37.2	30.7	0	112.59	585.05	3.3	45.5	5.4	12.8	0	16.9	15.3	0
62.87	399.82	5.3	18.8	2.9	10.6	0.5	29.5	25.6	1.4	113.09	587.03	1.2	40.9	7.0	12.8	1.2	16.3	20.2	0
63.97	402.72	19.0	7.1	3.8	9.0	0	21.4	38.6	0	114.09	591.00	1.5	41.8	0	0.4	0	53.7	2.2	0
65.46	406.66	14.5	17.5	6.5	3.5	3.0	20.0	32.5	0	114.59	592.98	0	50.7	0	1.5	0	45.9	2.0	0
66.95	410.59	29.7	24.3	3.5	3.5	0.5	14.4	20.3	0	115.09	594.96	0.8	54.2	1.5	1.9	0	32.6	7.6	0
68.44	414.52	2.2	3.5	4.8	5.7	0	43.4	40.4	0	117.09	602.89	2.1	24.1	11.6	12.9	0	34.4	14.5	0
69.44	417.16	7.0	13.4	7.0	11.9	0	17.9	41.3	0	118.59	608.84	5.8	9.3	10.4	16.6	0	17.4	39.8	0.4
70.43	419.78	14.6	16.9	10.0	14.2	0	24.9	18.0	0.8	119.08	610.78	6.3	4.9	10.7	3.9	0	43.9	28.8	0
70.93	421.10	10.8	3.3	16.9	0.9	4.2	37.6	23.9	0	119.58	612.77	7.8	5.0	30.1	11.4	0.9	27.4	16.0	0
72.43	432.90	0	3.8	1.1	0.0	0	91.0	3.4	0	123.07	653.89	0.4	2.9	0.8	0.8	0	90.1	2.9	0.4
75.29	480.66	6.1	15.0	16.8	1.9	0.9	20.1	32.2	1.9	124.57	676.66	4.7	23.8	9.8	8.9	0.5	30.4	21.0	0
75.79	484.38	10.9	13.9	9.7	4.1	0	13.1	45.3	0	125.42	688.26	1.2	13.4	4.3	2.0	0.4	72.3	5.5	0
76.79	486.23	5.3	18.9	9.5	11.9	0.4	32.5	20.2	0	125.92	691.55	2.5	5.8	6.3	2.9	0	67.1	14.6	0
79.79	491.78	14.9	15.4	5.0	7.1	0	19.1	34.0	1.2	126.92	695.56	2.3	12.1	6.0	21.4	0	15.8	40.5	0
81.29	494.55	7.9	26.9	11.5	9.5	0	15.0	27.7	0.4	127.42	697.57	7.1	14.2	9.0	21.8	0.9	20.4	22.3	0
82.27	496.36	5.7	22.6	10.8	18.9	0.5	17.5	22.2	0	128.92	703.60	3.5	12.2	9.6	18.7	0.9	26.1	28.7	0
83.77	499.14	10.2	33.3	10.6	7.9	0.5	19.9	10.6	0.5	130.24	708.91	0.9	20.8	7.9	6.9	0	36.6	25.0	0
84.27	500.06	15.2	34.8	7.0	4.3	0.9	27.0	10.0	0	131.24	717.63	0	0	0.4	0	0	95.8	3.9	0
88.48	507.84	10.0	11.3	4.3	10.0	0	22.5	39.0	0.4	131.73	720.68	0.4	0.7	0	0	0	94.1	3.7	0
88.97	508.75	6.6	33.8	7.5	7.0	0	8.5	33.3	0	132.23	723.80	0.4	0.7	0	0	0	94.1	4.8	0
91.96	514.28	12.0	22.4	7.5	13.7	1.7	9.1	30.3	0	133.22	729.08	7.2	14.0	2.7	9.0	0	32.6	33.9	0
92.46	515.20	15.6	21.3	9.5	8.1	0.9	16.6	21.8	0	134.22	732.43	2.8	16.8	8.4	10.5	0.7	31.6	27.4	0
93.82	517.72	16.7	29.2	8.2	6.4	0	15.0	23.2	0	135.29	736.02	0.9	18.5	6.5	2.8	0	60.2	11.1	0
94.82	519.56	20.2	21.0	2.9	6.7	0	36.1	9.2	0.4	135.79	737.69	5.4	25.4	6.5	2.2	0	33.7	22.5	0
96.17	522.06	0.4	27.8	0.4	0.4	0	63.5	6.5	0	136.29	739.37	3.1	19.5	6.2	6.2	0	44.0	19.5	0
96.67	522.99	1.8	28.3	0	0	0	68.2	0.4	0	138.29	763.73	3.5	12.9	3.5	3.5	0.5	56.2	18.9	0
97.17	523.91	0.4	24.5	0	1.2	0	68.0	3.6	0	139.29	775.66	3.9	6.1	2.6	0.4	0	60.0	26.1	0
98.17	525.76	0	27.2	1.0	1.0	0	65.8	5.0	0	139.79	781.63	4.5	1.5	3.0	4.9	0	25.9	58.6	0
99.17	527.61	0.4	24.5	0.8	0	0	67.2	5.5	0	140.29	787.59	7.4	10.3	7.4	13.2	2.6	9.2	46.0	0
100.18	529.47	0	29.8	0	0	0	65.9	3.9	0	141.44	802.26	0.5	4.7	0	0	0	89.3	5.6	0
100.68	530.40	1.8	26.0	0	0.4	0	68.6	0.9	0	141.93	808.94	3.1	51.2	4.3	2.3	1.2	33.7	4.3	0
101.18	532.90	0	40.3	0	0.9	0	55.8	2.2	0	142.93	822.51	2.0	14.8	1.2	2.0	1.6	71.3	6.1	0

Appendix 1. *Continued.*

	No.	1	2	3	4	5	6	7	8		No.	1	2	3	4	5	6	7	8
143.43	826.48	0.0	31.9	1.0	0	0.5	62.3	3.4	0	186.58	1162.79	0.5	8.1	26.7	3.2	0	53.4	6.8	0
143.93	830.06	1.5	43.9	0.7	0	0.4	41.6	11.5	0	188.08	1191.42	1.8	14.0	6.8	3.2	3.2	52.3	18.0	0
144.43	833.64	8.5	28.5	1.6	1.6	1.2	29.3	26.0	0	188.95	1208.95	0	15.8	3.7	3.7	0.9	68.8	2.8	0
144.92	837.15	10.8	30.0	7.5	7.5	0.5	18.3	23.0	0	189.58	1212.63	2.1	19.4	4.2	3.8	0.4	64.1	5.5	0
145.42	840.96	3.2	34.1	2.0	1.2	0	52.8	6.3	0	190.08	1214.03	5.1	7.4	2.8	8.3	2.3	69.6	3.2	0
146.27	848.12	2.3	8.0	1.4	0	0	80.3	4.7	0	191.08	1216.90	1.9	21.9	1.9	0	0	70.0	3.8	0
147.27	856.55	3.6	26.0	3.1	1.3	0.9	40.8	23.3	0	192.58	1224.86	3.5	27.4	1.7	4.9	0.9	5.2	51.0	0
147.77	860.77	6.5	5.6	2.6	4.7	1.7	62.9	14.7	0	195.08	1250.95	0	0	0	0	0	50.0	50.0	0
149.97	899.84	2.5	4.5	3.0	1.5	0	78.0	10.5	0	196.58	1270.23	0.0	94.7	0.4	0	0	2.5	2.1	0
150.96	904.32	1.6	7.5	4.4	12.3	0.4	63.9	8.7	0.4	197.58	1278.58	0.5	96.8	0	0	0	0.5	1.8	0
151.46	906.39	0.7	9.1	3.3	2.6	1.5	65.3	16.4	0.7	198.58	1285.62	0.0	90.7	0	0	0	2.9	5.9	0
152.45	910.49	5.0	12.0	4.5	5.5	0.5	48.0	21.0	0.5	200.04	1292.48	0.0	54.5	6.8	5.2	0	4.7	15.2	0
152.95	912.56	4.3	15.5	3.0	4.3	0.9	58.8	12.4	0	201.54	1297.88	0.8	53.8	4.6	8.8	0.8	2.9	21.8	0
154.95	926.67	1.4	1.4	0.9	0	0	94.5	1.8	0	202.54	1300.55	2.5	13.9	4.0	6.9	1.0	2.0	65.8	0
155.45	931.25	1.2	4.0	0.8	0	1.2	88.3	4.0	0	204.54	1305.98	3.3	26.7	5.2	26.7	0	2.2	26.3	1.9
156.13	937.49	4.5	13.1	8.2	7.2	1.4	54.0	11.7	0	206.04	1325.48	2.4	57.2	1.2	22.4	0.4	1.2	14.4	0
156.45	940.42	0.5	0	0.5	0	0	95.3	3.8	0	207.12	1333.99	2.1	23.5	2.5	30.9	0	2.5	31.7	0
156.63	942.07	0.9	0.9	0	0	0	94.6	3.6	0	207.54	1336.79	1.1	14.0	3.3	64.3	0.4	3.3	11.0	0
158.28	959.04	0.4	0.9	0	0.9	0	90.5	6.9	0	210.42	1351.35	2.3	23.9	3.2	15.8	0	8.6	32.4	0.5
159.28	967.12	2.4	9.2	0	0	0	79.6	5.3	0	212.44	1360.37	2.0	8.6	4.1	3.7	0	45.7	35.1	0
159.78	969.00	1.4	9.1	2.4	1.4	0	81.3	4.3	0	213.44	1373.07	1.6	23.2	3.2	1.6	0	54.0	8.0	0
160.28	970.88	0.4	2.6	0.4	0	0	94.8	1.5	0	214.94	1377.07	0.5	4.1	4.5	3.2	0	83.6	3.6	0.5
160.78	972.75	6.4	9.0	2.1	1.3	0	74.2	4.7	0	215.44	1378.40	2.2	6.1	10.1	7.0	0.4	57.0	14.5	0.9
161.29	974.67	2.4	6.1	3.3	0.8	0	80.8	6.5	0	216.94	1392.53	4.9	19.4	4.2	2.8	0	49.1	19.1	0
162.29	978.42	7.7	5.3	3.2	7.0	0.7	47.9	26.8	0	217.56	1400.06	0.4	47.8	0.4	0	0	48.7	1.3	0
163.79	988.54	5.1	17.0	1.6	1.6	0.4	69.2	4.0	0	219.05	1424.98	2.7	32.8	1.1	0.4	0.8	59.9	1.9	0
164.30	991.25	4.2	13.0	2.8	1.4	0.5	65.7	12.5	0	219.56	1435.17	4.6	17.4	4.6	11.4	0	45.7	13.2	0
165.80	997.53	3.2	12.2	4.5	1.4	0.5	58.8	15.8	0	220.56	1455.15	1.9	28.0	1.2	1.9	1.6	41.2	7.8	0
166.69	1022.82	2.4	3.3	1.4	0	0	88.0	3.8	0	222.06	1485.33	2.0	1.2	3.2	2.4	0	75.2	15.2	0
167.97	1033.56	3.2	12.8	4.1	2.7	0.5	62.1	11.4	0	223.56	1505.46	0.0	57.6	0.5	0	0	18.6	0.5	0
168.19	1034.44	2.3	11.8	5.9	5.0	0	66.1	7.7	0	224.81	1514.32	4.3	26.1	2.2	2.2	0	52.2	2.2	0
169.69	1040.45	6.0	31.7	4.0	3.6	0.4	44.2	7.6	0	226.31	1524.96	3.1	27.1	4.7	1.2	0	23.6	9.7	0
171.19	1046.46	2.2	31.2	3.7	4.1	0	54.6	3.0	0	228.21	1538.43	1.5	3.5	11.4	10.9	0	52.2	16.4	0
171.69	1048.24	4.1	20.6	5.0	2.8	0	60.6	5.0	0	228.65	1541.55	0.4	8.7	8.7	10.4	0	56.8	9.5	0
173.34	1052.51	1.4	19.4	1.8	1.8	0	66.7	6.3	0	230.15	1552.18	5.9	11.8	8.0	12.2	0	43.3	17.2	0
175.37	1060.73	7.0	11.6	2.8	3.7	0	65.1	5.6	0	231.65	1562.82	2.1	8.1	3.0	7.2	0	55.5	10.6	0
176.90	1077.57	6.6	21.0	8.2	10.7	0.8	33.7	17.3	0	232.15	1566.36	0.4	30.5	2.1	0	0	52.7	9.1	0
177.91	1087.72	5.0	11.5	2.3	4.6	0	74.8	0.8	0	233.15	1573.45	1.8	0.9	0.9	0	0	31.5	5.5	0
178.98	1098.26	4.2	13.2	4.2	4.7	0	47.2	23.6	0	234.15	1580.54	1.3	12.1	0.7	7.7	0	64.8	11.1	0
179.40	1102.53	3.0	5.5	0.8	3.8	0	81.8	3.0	0	235.01	1586.64	1.4	0.5	5.3	7.2	0	77.3	6.3	0
180.89	1111.95	2.3	17.3	6.8	12.7	0	51.8	7.7	0	236.01	1593.73	3.1	4.9	8.0	5.4	0	53.1	16.1	0
182.38	1118.16	2.8	14.1	5.6	13.6	0.5	56.8	5.6	0	237.01	1600.82	0.8	17.0	5.3	3.6	0.4	48.2	23.1	0.4
183.86	1136.72	1.7	6.7	0	2.5	0	74.4	14.3	0	238.00	1607.84	8.0	22.3	5.5	4.6	0.8	50.4	1.7	0
186.36	1159.68	1.4	4.1	0	0.5	0	88.0	5.1	0	238.01	1607.91	5.1	18.1	7.9	5.1	0.5	57.7	4.7	0

Appendix 2. Stable isotope data of foraminiferal shells.

	No.	1	2	3	4	5		No.	1	2	3	4	5
Depth (mcd)	Age (Ka) by Xuan *et al.* (2016)	*N. pachyderma* $\delta^{18}O$ (‰VPDB)	*T. quinqueloba* $\delta^{18}O$ (‰VPDB)	Difference $\delta^{18}O$ (‰VPDB)(*N. pachy–T. quin*)	No. of specimens; *N. pachyderma* (#)	No. of specimens; *T. quinqueloba* (#)	Depth (mcd)	Age (Ka) by Xuan *et al.* (2016)	*N. pachyderma* $\delta^{18}O$ (‰VPDB)	*T. quinqueloba* $\delta^{18}O$ (‰VPDB)	Difference $\delta^{18}O$ (‰VPDB)(*N. pachy–T. quin*)	No. of specimens; *N. pachyderma* (#)	No. of specimens; *T. quinqueloba* (#)
1.67	5.84	2.004	1.203	0.802	17	70	40.87	294.60	3.832	2.012	1.820	17	70
3.17	12.59	3.823	1.342	2.481	17	70	41.87	301.13	3.564	1.497	2.066	17	70
4.17	16.85	3.162	1.915	1.247	17	70	42.37	303.37	3.512	1.367	2.145	17	70
6.37	44.63	2.903	2.009	0.895	17	70	42.8	305.24	3.284	1.776	1.508	17	70
8.37	59.51	3.583	2.230	1.353	17	70	43.3	306.77	2.776	1.445	1.331	17	70
9.37	68.44	3.277	1.319	1.958	17	70	45.3	312.86	3.635	1.322	2.312	17	70
10.19	74.73	3.062	1.535	1.527	17	70	46.3	315.91	3.292	1.170	2.122	17	70
14.19	102.76	3.055	1.562	1.493	17	70	49.3	325.06	3.497	1.103	2.394	17	70
15.19	108.72	2.842	–	–	17	–	50.43	328.50	2.885	0.819	2.065	17	70
17.69	114.68	2.980	1.987	0.992	17	70	51.43	331.55	2.509	1.167	1.342	17	70
21.19	122.23	2.475	–	–	17	–	52.43	344.75	4.361	2.748	1.613	17	70
23.74	156.31	4.097	2.665	1.432	17	70	53.43	362.65	3.803	2.450	1.353	17	70
26.24	194.05	3.702	1.441	2.261	17	70	54.26	374.98	2.982	1.761	1.221	17	70
26.86	198.00	2.668	1.485	1.182	17	70	54.76	376.49	3.198	2.505	0.692	17	70
27.36	201.19	2.870	1.622	1.248	17	70	55.26	378.00	3.055	2.231	0.825	17	70
28.86	208.29	2.456	1.565	0.891	17	70	55.76	379.51	2.733	2.030	0.703	17	70
30.86	216.26	2.762	1.638	1.124	17	70	56.26	381.02	2.603	1.538	1.064	17	70
33.36	235.61	3.529	0.654	2.875	17	70	56.76	382.53	2.893	2.014	0.879	17	70
36.66	262.32	3.300	1.710	1.589	17	70	57.26	384.04	2.515	1.950	0.566	17	70
37.66	271.73	3.948	2.643	1.305	17	70	57.76	385.54	2.767	1.815	0.953	17	70
38.16	276.43	4.154	3.119	1.035	17	70	58.26	387.05	2.632	2.136	0.496	17	70
38.87	281.32	3.136	1.919	1.216	17	70	59.26	390.07	3.237	1.539	1.698	17	70
39.87	287.83	3.239	1.863	1.376	17	70	61.37	395.86	1.885	1.633	0.251	17	70
40.37	291.09	3.333	1.807	1.526	17	70	62.37	398.50	–	1.393	–	–	70

Appendix 2. *Continued.*

	No.	1	2	3	4	5		No.	1	2	3	4	5
65.46	406.66	3.515	1.668	1.847	17	70	143.43	826.48	2.835	2.134	0.701	17	70
70.43	419.78	2.917	1.772	1.145	17	70	143.93	830.06	2.547	2.089	0.458	17	70
76.79	486.23	2.251	1.664	0.586	17	70	147.27	856.55	1.702	1.652	0.050	17	70
81.29	494.55	2.352	1.500	0.852	17	70	151.46	906.39	2.144	1.558	0.586	17	69
84.27	500.06	2.906	2.054	0.852	17	70	152.95	912.56	1.295	1.520	−0.225	17	70
88.97	508.75	2.758	1.693	1.065	17	70	156.13	937.49	2.038	1.622	0.416	17	70
91.96	514.28	3.113	1.477	1.636	17	70	160.78	972.75	2.838	–	–	17	–
94.82	519.56	2.427	–	–	17	–	164.3	991.25	2.991	1.807	1.183	17	70
96.17	522.06	4.121	3.282	0.839	17	70	168.19	1034.44	2.714	1.860	0.854	15	70
98.17	525.76	3.439	2.934	0.505	17	70	171.19	1046.46	2.791	1.906	0.885	17	70
99.17	527.61	3.375	3.119	0.256	17	70	176.9	1077.57	2.116	1.603	0.513	17	70
100.18	529.47	3.093	3.172	−0.079	17	70	177.91	1087.72	2.468	1.882	0.586	17	70
100.68	530.40	3.013	3.091	−0.078	17	70	180.89	1111.95	2.506	1.590	0.917	17	70
101.68	536.37	3.157	2.958	0.199	17	70	183.86	1136.72	3.348	1.950	1.398	17	70
102.67	543.23	3.512	3.218	0.294	17	70	186.58	1162.79	1.714	1.641	0.073	17	70
104.87	555.54	2.951	2.666	0.285	17	70	188.08	1191.42	1.811	1.638	0.174	17	70
105.87	559.12	2.906	2.468	0.438	17	70	189.58	1212.63	2.419	2.121	0.297	17	70
108.86	569.81	2.175	0.967	1.208	17	70	191.08	1216.90	2.458	2.495	−0.037	17	70
110.86	576.97	1.514	1.606	−0.092	17	70	192.58	1224.86	1.891	1.746	0.145	17	70
111.87	581.64	3.409	2.564	0.845	17	70	197.58	1278.58	–	2.905	–	–	70
114.09	591.00	2.665	2.587	0.078	17	70	201.54	1297.88	–	2.314	–	–	70
117.09	602.89	2.534	1.505	1.028	17	70	206.04	1325.48	–	2.751	–	–	70
118.59	608.84	3.231	1.554	1.677	17	70	212.44	1360.37	1.667	1.238	0.429	17	70
124.57	676.66	1.896	1.550	0.346	17	70	216.94	1392.53	2.101	1.993	0.107	17	70
125.42	688.26	2.674	1.756	0.917	17	70	220.56	1455.15	2.954	–	–	17	–
130.24	708.91	2.972	1.588	1.385	17	70	226.31	1524.96	2.496	2.272	0.224	17	60
134.22	732.43	2.374	1.643	0.731	17	70	228.65	1541.55	2.577	2.419	0.158	17	70
135.29	736.02	2.966	2.218	0.747	17	70	231.65	1562.82	2.474	2.128	0.347	17	54
136.29	739.37	2.589	1.938	0.650	17	70	237.01	1600.82	2.434	1.943	0.491	17	70
138.29	763.73	2.288	2.030	0.258	17	70	238.01	1607.91	2.457	2.133	0.324	17	70
142.93	822.51	2.931	1.638	1.293	17	70							

Appendix 3. Morphometric data of *Neogloboquadrina pachyderma*.

	No.	1	2	3	4	5	6	7	8	9	10	11	12	13
Depth (mcd)	Age (Ka) by Xuan *et al.* (2016)	Area (μm^2)	Perimeter (μm)	Diameter Max (μm)	Diameter Min (μm)	ECD* (μm)	Sphericity	Aspect Ratio	Elongation	Convexity	Shape Factor	Principal component 1†	Principal component 2‡	Number of specimens (#)
1.67	5.84	30877.90	632.83	216.13	179.79	193.48	0.76	1.16	1.16	0.98	0.93	−0.26	−0.11	9
3.17	12.59	44785.87	758.88	256.13	219.11	233.27	0.75	1.15	1.16	0.98	0.93	−0.04	−0.14	25
3.87	15.64	48384.31	793.68	267.04	230.25	244.62	0.78	1.14	1.14	0.98	0.94	0.24	−0.17	95
4.17	16.85	44918.26	776.20	261.12	220.96	235.30	0.77	1.15	1.15	0.97	0.91	−0.54	−0.36	83
6.37	44.63	51521.03	823.76	278.97	235.99	252.06	0.75	1.16	1.16	0.98	0.92	−0.22	0.03	40
8.37	59.51	43897.60	757.16	256.03	218.30	232.87	0.75	1.15	1.16	0.98	0.93	0.05	0.07	80
10.69	78.54	40553.05	727.69	246.88	210.09	224.38	0.75	1.15	1.16	0.98	0.94	0.21	0.13	174
12.69	92.02	46659.91	777.47	264.11	224.02	239.87	0.75	1.16	1.16	0.98	0.94	0.16	0.17	241
14.19	102.76	37158.70	694.63	235.78	201.68	214.48	0.75	1.15	1.16	0.98	0.94	0.18	0.12	131
16.69	112.42	33709.37	662.74	226.91	190.79	204.06	0.73	1.17	1.18	0.98	0.94	−0.03	0.32	37
23.74	156.31	52420.14	827.32	278.37	239.82	254.38	0.77	1.14	1.15	0.98	0.94	0.18	−0.09	152
26.24	194.05	37968.69	704.59	235.43	205.31	215.08	0.80	1.12	1.12	0.98	0.92	−0.16	−0.81	15
30.86	216.26	34718.52	698.31	227.42	195.61	204.58	0.79	1.13	1.13	0.96	0.85	−1.94	−1.73	18
33.36	235.61	42301.64	766.61	252.24	214.72	228.03	0.75	1.16	1.16	0.97	0.88	−1.13	−0.59	13
38.16	276.43	44942.62	771.77	260.24	222.50	236.81	0.76	1.15	1.15	0.98	0.93	0.05	−0.07	218
40.37	291.09	43333.92	748.25	254.78	218.04	232.44	0.76	1.15	1.15	0.98	0.95	0.56	0.25	214
42.37	303.37	39280.82	718.01	242.94	207.57	220.44	0.76	1.14	1.15	0.98	0.93	−0.03	−0.18	107
52.43	344.75	45941.05	779.45	262.67	226.31	239.53	0.78	1.14	1.14	0.98	0.93	0.09	−0.18	191
54.76	376.49	39335.75	724.93	244.88	207.13	220.39	0.75	1.16	1.16	0.98	0.92	−0.46	−0.18	158
55.76	379.51	33845.28	680.90	229.32	193.31	204.74	0.72	1.17	1.18	0.97	0.90	−1.07	−0.39	88
58.26	387.05	38118.07	726.31	243.15	205.67	217.08	0.73	1.17	1.17	0.97	0.88	−1.36	−0.61	109
61.37	395.86	23710.32	562.31	191.04	162.94	172.46	0.76	1.14	1.15	0.97	0.93	−0.23	−0.33	114
62.37	398.50	23191.22	562.28	191.28	161.30	170.71	0.74	1.16	1.17	0.97	0.91	−0.70	−0.43	82
63.97	402.72	25736.44	584.10	199.45	169.32	179.44	0.76	1.14	1.15	0.98	0.93	−0.13	−0.28	44
65.46	406.66	24914.55	573.02	195.29	167.23	176.58	0.76	1.14	1.15	0.98	0.94	−0.05	−0.30	45
66.95	410.59	25600.60	585.94	199.75	167.38	178.43	0.75	1.16	1.16	0.97	0.92	−0.58	−0.23	97
68.44	414.52	23882.42	564.94	192.82	163.21	173.40	0.75	1.16	1.16	0.98	0.93	−0.24	−0.12	98
69.44	417.16	27998.25	607.83	207.65	175.15	187.20	0.74	1.16	1.17	0.98	0.94	−0.06	0.06	36
70.43	419.78	26477.90	595.25	203.74	171.08	182.03	0.73	1.16	1.18	0.97	0.92	−0.51	−0.13	64

Appendix 3. *Continued.*

	No.	1	2	3	4	5	6	7	8	9	10	11	12	13
72.43	432.90	35513.23	676.29	229.66	199.19	210.78	0.78	1.13	1.14	0.98	0.96	0.75	0.09	239
75.79	484.38	32209.80	648.11	221.67	188.20	200.57	0.75	1.15	1.16	0.98	0.95	0.26	0.17	34
76.79	486.23	30483.93	630.87	216.77	181.92	194.81	0.73	1.17	1.18	0.98	0.94	0.06	0.28	84
81.29	494.55	37092.95	689.73	235.60	199.34	213.18	0.75	1.15	1.16	0.98	0.94	0.22	0.11	38
82.27	496.36	43445.78	745.69	254.19	216.06	229.69	0.75	1.15	1.16	0.98	0.94	0.11	0.06	37
84.27	500.06	34338.83	666.53	228.56	192.48	205.89	0.73	1.16	1.17	0.98	0.94	0.14	0.21	61
88.97	508.75	29734.26	623.94	212.15	181.55	191.95	0.79	1.13	1.13	0.98	0.94	−0.03	−0.45	18
91.96	514.28	36681.44	690.53	234.73	199.35	212.46	0.75	1.15	1.16	0.98	0.94	0.00	−0.03	22
93.82	517.72	37141.49	695.98	237.60	199.91	213.72	0.73	1.16	1.17	0.98	0.93	−0.13	0.08	35
94.82	519.56	37598.71	697.51	238.90	201.45	215.40	0.73	1.17	1.18	0.98	0.94	0.14	0.39	101
96.17	522.06	40503.21	723.03	245.66	211.21	224.06	0.77	1.14	1.15	0.98	0.95	0.45	0.00	146
97.17	523.91	37173.05	692.57	236.34	201.48	214.19	0.75	1.15	1.16	0.98	0.95	0.28	0.20	172
98.17	525.76	38524.31	703.26	240.51	204.04	217.70	0.75	1.15	1.16	0.98	0.95	0.35	0.23	147
99.17	527.61	41066.61	724.99	247.40	210.94	224.54	0.75	1.15	1.16	0.98	0.95	0.39	0.19	165
100.18	529.47	37633.61	696.73	238.88	201.62	215.62	0.73	1.16	1.17	0.98	0.95	0.29	0.36	135
100.68	530.40	45625.64	768.82	261.79	223.24	237.66	0.76	1.15	1.15	0.98	0.94	0.30	0.06	153
101.68	536.37	48119.58	785.82	268.54	226.50	242.35	0.73	1.16	1.17	0.98	0.94	0.13	0.27	161
102.67	543.23	37949.56	701.17	239.27	203.43	216.84	0.75	1.15	1.16	0.98	0.95	0.30	0.20	185
103.67	550.17	34814.55	670.01	229.37	194.92	207.75	0.75	1.15	1.16	0.98	0.95	0.40	0.24	180
104.87	555.54	29930.22	623.20	213.32	181.04	193.18	0.75	1.15	1.16	0.98	0.95	0.35	0.19	113
105.87	559.12	29102.87	615.48	210.53	179.32	190.66	0.75	1.15	1.16	0.98	0.95	0.32	0.14	118
108.86	569.81	25760.85	582.18	197.77	169.79	180.05	0.78	1.13	1.14	0.98	0.95	0.28	−0.20	37
109.86	573.39	26542.76	593.82	203.38	171.58	182.84	0.73	1.16	1.18	0.98	0.94	−0.07	0.15	35
110.86	576.97	25067.20	572.09	196.60	166.43	177.50	0.75	1.15	1.16	0.98	0.95	0.39	0.17	42
111.87	581.64	35309.45	671.96	228.57	196.51	207.89	0.76	1.14	1.15	0.98	0.95	0.36	0.04	134
112.59	585.05	29280.09	620.03	212.42	179.29	191.24	0.73	1.16	1.18	0.98	0.94	0.08	0.18	40
113.09	587.03	26864.78	591.59	201.02	172.56	182.65	0.76	1.14	1.15	0.98	0.94	0.12	−0.15	42
114.09	591.00	26677.28	585.88	199.96	170.82	181.91	0.76	1.14	1.15	0.98	0.95	0.45	0.11	142
115.09	594.96	28576.62	605.90	208.22	175.52	187.92	0.74	1.16	1.17	0.98	0.95	0.34	0.43	85
117.09	602.89	27348.38	596.66	204.15	174.18	184.92	0.76	1.14	1.15	0.98	0.95	0.34	−0.01	83
118.59	608.84	26322.63	587.45	201.80	169.26	181.49	0.72	1.17	1.18	0.98	0.94	0.11	0.33	45
119.58	612.77	27085.91	594.39	204.05	171.88	183.57	0.73	1.16	1.18	0.98	0.94	0.09	0.21	60
124.57	676.66	29876.81	623.80	212.80	181.39	192.31	0.76	1.15	1.16	0.98	0.94	0.08	−0.10	65
125.42	688.26	31210.91	637.34	218.27	184.72	196.96	0.75	1.15	1.16	0.98	0.94	0.21	0.09	182
125.92	691.55	28024.48	604.67	207.19	175.27	186.68	0.73	1.16	1.18	0.98	0.94	0.07	0.15	165
126.92	695.56	30572.02	630.01	215.36	183.31	194.47	0.75	1.15	1.17	0.98	0.94	0.08	0.05	34

Appendix 3. *Continued.*

	No.	1	2	3	4	5	6	7	8	9	10	11	12	13
128.92	703.60	32064.47	647.16	221.04	185.94	199.17	0.73	1.16	1.17	0.98	0.94	−0.02	0.18	60
130.24	708.91	30551.78	628.88	215.43	181.93	194.18	0.74	1.16	1.17	0.98	0.94	0.09	0.17	79
131.24	717.63	34124.87	661.93	224.46	194.85	206.52	0.78	1.13	1.14	0.99	0.96	0.81	0.12	251
132.23	723.80	38186.36	697.83	237.21	204.58	217.37	0.77	1.14	1.14	0.98	0.96	0.73	0.14	249
133.22	729.08	30845.79	633.26	217.35	182.56	195.27	0.73	1.16	1.18	0.98	0.94	0.02	0.23	83
134.22	732.43	31404.96	638.05	218.50	185.36	196.91	0.74	1.15	1.17	0.98	0.94	0.10	0.10	89
135.29	736.02	34585.86	668.79	227.76	194.17	205.98	0.74	1.15	1.17	0.98	0.94	0.04	0.05	129
136.29	739.37	34934.83	672.94	229.41	194.39	207.32	0.75	1.16	1.17	0.98	0.94	0.01	0.06	114
138.29	763.73	26877.61	592.34	202.37	172.36	183.66	0.75	1.15	1.16	0.98	0.95	0.34	0.11	110
139.29	775.66	31394.90	639.16	218.20	185.47	197.23	0.76	1.14	1.15	0.98	0.94	0.14	−0.08	134
139.79	781.63	28672.54	612.29	210.54	176.59	189.00	0.72	1.17	1.19	0.98	0.94	0.04	0.38	70
141.44	802.26	35769.00	678.77	230.88	198.55	210.41	0.76	1.14	1.15	0.98	0.95	0.46	0.04	189
141.93	808.94	29247.20	616.16	210.86	178.65	189.89	0.73	1.16	1.18	0.98	0.94	−0.03	0.14	84
142.93	822.51	33839.71	662.78	226.17	193.18	204.92	0.75	1.15	1.16	0.98	0.94	0.26	0.05	173
143.43	826.48	30202.73	629.72	215.58	182.61	194.50	0.74	1.16	1.17	0.98	0.94	0.18	0.18	130
143.93	830.06	26247.63	585.05	200.03	170.47	181.29	0.76	1.14	1.15	0.98	0.95	0.34	0.00	112
144.92	837.15	30775.37	635.45	217.56	182.61	194.49	0.72	1.16	1.18	0.97	0.93	−0.35	−0.02	38
145.42	840.96	29678.54	623.18	215.01	179.47	191.91	0.71	1.17	1.19	0.98	0.94	−0.09	0.35	132
146.27	848.12	31722.76	646.70	222.56	185.35	198.38	0.71	1.18	1.19	0.98	0.93	−0.26	0.30	175
147.27	856.55	31393.68	644.95	220.04	185.60	197.57	0.73	1.16	1.18	0.97	0.93	−0.36	−0.12	90
147.77	860.77	32620.08	656.68	224.16	189.23	201.36	0.73	1.16	1.18	0.98	0.93	−0.22	−0.01	151
149.97	899.84	41821.67	734.93	249.64	214.14	227.24	0.76	1.14	1.15	0.98	0.95	0.34	0.00	152
150.96	904.32	36839.63	691.85	235.55	200.20	212.60	0.75	1.15	1.16	0.98	0.93	−0.08	−0.12	161
151.46	906.39	32170.46	648.49	221.61	188.23	199.80	0.75	1.15	1.17	0.98	0.94	−0.02	0.00	180
152.95	912.56	32022.32	647.54	221.50	186.70	198.78	0.74	1.16	1.17	0.98	0.93	−0.19	−0.09	131
154.95	926.67	42404.63	739.88	252.64	214.86	228.09	0.75	1.15	1.17	0.98	0.94	0.14	0.09	206
155.45	931.25	38957.09	710.75	241.38	207.07	218.94	0.77	1.14	1.15	0.98	0.94	0.08	−0.22	217
156.13	937.49	37026.34	697.79	238.68	199.63	213.37	0.71	1.17	1.19	0.97	0.92	−0.44	0.01	159
156.63	942.07	43356.39	751.87	256.00	218.46	231.96	0.76	1.14	1.15	0.98	0.94	0.22	−0.11	211
158.28	959.04	37305.91	692.43	236.20	201.26	213.65	0.75	1.15	1.16	0.98	0.94	0.14	0.01	210
159.78	969.00	39749.09	719.52	245.39	208.88	221.60	0.75	1.15	1.16	0.98	0.94	0.05	0.00	173
160.28	970.88	41324.34	728.11	247.32	212.60	225.21	0.77	1.14	1.15	0.98	0.95	0.36	−0.08	249
160.78	972.75	42066.96	740.40	252.79	213.66	228.03	0.74	1.16	1.17	0.98	0.94	0.05	0.11	173
161.29	974.67	39336.53	713.13	243.58	206.82	220.03	0.74	1.15	1.17	0.98	0.94	0.13	0.12	198
162.29	978.42	34046.73	663.86	227.33	192.64	204.93	0.74	1.16	1.17	0.98	0.94	0.12	0.17	136
164.3	991.25	34683.08	667.20	227.75	193.36	205.36	0.75	1.15	1.16	0.98	0.94	−0.02	−0.07	141

Appendix 3. *Continued.*

	No.	1	2	3	4	5	6	7	8	9	10	11	12	13
166.69	1022.82	42081.75	737.93	251.82	213.49	226.69	0.74	1.15	1.17	0.98	0.93	−0.12	−0.09	181
168.19	1034.44	33641.87	661.98	226.43	190.84	202.80	0.73	1.16	1.18	0.98	0.93	−0.32	0.01	143
171.19	1046.46	38320.96	699.98	238.60	202.39	215.71	0.75	1.15	1.16	0.98	0.94	0.09	0.03	146
176.9	1077.57	30790.21	639.66	218.34	184.39	195.85	0.73	1.16	1.18	0.97	0.93	−0.36	−0.15	74
177.91	1087.72	37913.01	701.57	239.51	202.12	215.05	0.73	1.16	1.18	0.98	0.93	−0.24	−0.02	201
180.89	1111.95	35141.23	677.85	231.21	196.19	208.27	0.75	1.16	1.17	0.98	0.93	−0.11	−0.02	109
183.86	1136.72	34265.68	667.38	227.62	193.52	205.90	0.76	1.15	1.16	0.98	0.94	0.16	0.04	172
186.58	1162.79	32784.44	658.37	224.19	190.93	201.93	0.75	1.14	1.16	0.98	0.93	−0.16	−0.27	117
188.08	1191.42	29266.46	620.19	211.74	179.57	190.65	0.75	1.15	1.16	0.98	0.93	−0.10	−0.15	110
189.58	1212.63	29183.74	623.52	213.93	179.01	190.87	0.73	1.16	1.18	0.97	0.93	−0.36	−0.02	143
191.08	1216.90	25376.34	585.12	200.58	168.27	178.73	0.73	1.16	1.18	0.97	0.92	−0.56	−0.19	138
192.58	1224.86	24141.48	578.13	200.51	165.14	175.13	0.67	1.20	1.23	0.97	0.91	−1.14	0.11	18
200.04	1292.48	25141.30	575.36	197.89	166.35	176.56	0.74	1.16	1.17	0.98	0.94	−0.15	0.05	9
201.54	1297.88	26851.69	604.06	206.55	173.30	184.35	0.74	1.15	1.16	0.97	0.92	−0.46	−0.40	7
206.04	1325.48	30211.35	633.08	215.83	183.03	195.53	0.74	1.15	1.16	0.98	0.94	0.16	0.11	3
207.54	1336.79	29173.42	616.53	208.09	181.50	191.46	0.78	1.13	1.14	0.98	0.95	0.44	−0.17	9
210.42	1351.35	39248.97	727.88	246.11	209.54	219.92	0.73	1.16	1.18	0.97	0.90	−1.09	−0.64	19
212.44	1360.37	30288.14	632.13	215.90	181.51	193.98	0.74	1.16	1.17	0.98	0.93	−0.21	0.02	109
214.94	1377.07	30096.42	631.11	216.20	182.01	193.88	0.73	1.16	1.18	0.98	0.93	−0.16	0.06	183
216.94	1392.53	33153.13	661.63	226.99	190.73	203.03	0.73	1.16	1.18	0.98	0.93	−0.19	0.07	139
219.05	1424.98	28399.78	615.30	211.80	177.08	188.58	0.72	1.17	1.19	0.97	0.93	−0.34	0.08	154
220.56	1455.15	27426.55	601.93	207.35	174.41	185.35	0.72	1.17	1.19	0.98	0.94	−0.10	0.21	104
222.06	1485.33	25397.01	582.53	199.64	168.15	178.77	0.74	1.16	1.17	0.97	0.93	−0.27	−0.15	187
224.81	1514.32	32122.45	649.21	221.47	189.99	200.16	0.78	1.13	1.14	0.98	0.94	0.12	−0.46	24
226.31	1524.96	32555.31	655.18	223.70	189.02	200.67	0.75	1.15	1.16	0.98	0.93	−0.27	−0.18	60
228.65	1541.55	28725.02	617.56	211.62	178.01	189.64	0.73	1.16	1.18	0.98	0.93	−0.22	−0.04	137
231.65	1562.82	27738.47	604.92	206.59	175.73	186.33	0.75	1.15	1.16	0.98	0.94	0.02	−0.09	131
233.15	1573.45	29436.04	621.24	212.24	180.69	191.68	0.76	1.14	1.16	0.98	0.94	0.14	−0.18	68
235.01	1586.64	27937.35	605.90	207.95	174.47	186.95	0.73	1.16	1.18	0.98	0.94	0.03	0.21	155
237.01	1600.82	27356.54	603.25	206.26	174.27	184.80	0.73	1.16	1.18	0.97	0.93	−0.34	−0.10	118
238.01	1607.91	30495.92	634.23	217.18	183.10	195.07	0.74	1.16	1.17	0.98	0.93	−0.10	0.02	121

* Equivalent Circle Diameter

† Aspectratio shapefactor covexcity

‡ Aspectratio shapefactor covexcity